THE IMPACT OF GLOBAL OCEAN/ATMOSPHERE COUPLING ON NH ENSO VARIABILITY : SENSITIVITY TO CONVECTION IN THE TROPICAL NORTHWEST PACIFIC

(Submitted to Journal of Climate)

July 2006

Ileana Bladé [1], Matthew Newman [2], Michael A. Alexander [3] and James D. Scott [2]

1. Departament d'Astronomia i Meteorologia, Universitat de Barcelona, Spain.
2. CIRES Climate Diagnostics Center, University of Colorado, and Physical Sciences Division/NOAA Earth System Research Laboratory, Boulder, Colorado.
3. Physical Sciences Division/NOAA Earth System Research Laboratory, Boulder, Colorado.

Corresponding author address: Dr. Ileana Bladé, Departament d'Astronomia i Meteorologia, Facultat de Fisica, Av. Diagonal 647, 08028 Barcelona. SPAIN. Email: ileanablade@ub.edu

Abstract

This paper examines the influence of tropical and global ocean/atmosphere coupling on the NH extratropical atmospheric response to the 1997/98 El Niño and 1998/99 La Niña events, using very large ensembles (either 100 or 150 members) of coupled and uncoupled GCM simulations. In all model simulations, observed sea surface temperatures (SST) are prescribed in the tropical eastern Pacific. In the control simulations, climatological SSTs are specified elsewhere, whereas in the coupled simulations a bulk mixed layer model is coupled to the atmosphere in the Indo-Western Pacific ocean or in the entire ocean.

Most of the impact of global air/sea interactions on the ENSO response in this model can be attributed to coupling in the Tropics, which acts to amplify the ENSO teleconnection, with extratropical coupling exerting a weaker counteracting damping effect. The enhancement of the ENSO teleconnection due to tropical coupling is particularly pronounced in early winter of the Niño year, but is absent in midwinter of that same year. Chiefly, this effect is due to an increase, in both the mean and variance, of convection in a small area of the tropical northwest Pacific (TNWP), which occurs via enhanced evaporation associated with a slightly warmer coupled western Pacific. These changes in tropical convection can significantly affect the early winter extratropical Niño response because the PNA region is very sensitive to TNWP forcing at this time, when the Pacific jet is relatively weak and steers the Rossby wavetrain emanating from the TNWP region towards the PNA region. Because this wavetrain interferes constructively with the main ENSO wavetrain emanating from the central equatorial Pacific, the coupled extratropical response to ENSO is amplified. Analogous (but opposite and weaker) results apply throughout the Niña winter. In midwinter of the El Niño year, however, when the Pacific jet is stronger and there is strong mean subsidence in the TNWP region, Rossby waves emanating from this region are trapped in the

subtropics and coupling has little impact on TNWP convection or on the ENSO response.

Observational evidence supports the existence of a preferred region in the tropical northwest Pacific for forcing PNA circulation anomalies in the PNA sector in early winter. Thus, how convection in that region is affected by interactions with the ocean may well play an important role in driving ENSO teleconnections. Additionally, the impact of coupling on ENSO variability may be very dependent on month-to-month changes in the background state.

1. Introduction

The strongest potentially predictable interannual signal in many extratropical regions is that forced by tropical Pacific SST anomalies associated with the El Niño/Southern Oscillation (ENSO). As models of the coupled tropical system continue to become more sophisticated and effective at forecasting the state of the equatorial Pacific a few seasons and even a year in advance (Palmer et al. 2004), one can expect that seasonal prediction of the most robust remote manifestations of ENSO will also become feasible. Successful modeling and prediction of these atmospheric ENSO teleconnections, however, requires progress along many fronts, among which is improved understanding of the direct and indirect mechanisms involved in the generation and maintenance of this remote ENSO response and its relation to tropical convection.

One plausible way of fine-tuning the simulation and/or increasing the predictability of ENSO extratropical teleconnections is to allow air/sea interactions outside the tropical eastern Pacific. To ensure realistic SST forcing, modeling studies have traditionally considered the atmospheric response to prescribed SST boundary conditions in the tropical Pacific (TOGA-type experiments) or worldwide (GOGA or AMIP-type experiments). Yet ENSO forces global oceanic as well as atmospheric teleconnections by inducing remote near-surface temperature, humidity and wind fluctuations along with cloud cover changes, which in turn modify the fluxes of heat and momentum at the ocean interface and generate SST anomalies — a mechanism known as the "atmospheric bridge" (Alexander 1992a, Luksch and von Storch 1992, Lau and Nath 1996. See also the review by Alexander et al. 2002). It is conceivable that some of these SST anomalies could then feedback onto the atmospheric ENSO response, both locally and remotely.

These feedbacks can easily be incorporated into a GCM by coupling it to a mixed-layer ocean model outside the tropical Pacific. This approach, in which tropical Pacific SSTs are prescribed from observations or "pre-forecasts" but air/sea interaction is allowed in the remaining oceans, was originally devised in the early 1990s (Alexander 1992a,b) and is now becoming more commonly used in modeling and prediction studies (e.g., Huang et al. 2005, Seager 2006), sometimes under the name "pacemaker experiments"[1]. This strategy stems from increased awareness that AMIP or "two-tier"-type experiments, in which forcing is prescribed globally, fail to simulate variability in regions where atmospheric processes are crucial in determining SST anomalies. This problem is especially pronounced in the Indian Ocean, where clear skies lead to basin-wide oceanic warming during El Niño events, in nature and in coupled simulations, but where those same positive SSTs tend to excite convection in forced simulations (Kumar and Hoerling 1998; Krishna Kumar et al. 2005; Wang et al. 2006).

The importance of air/sea feedbacks for the *tropical* ENSO response has already been established. Lau and Nath (2000) and Alexander and Scott (2002) present modeling evidence that ENSO-induced SST anomalies contribute a negative feedback in the Indian Ocean and a positive feedback in the Caribbean region, respectively. Wang et al. (2000) have also suggested that strong thermodynamic air-sea interactions help maintain the surface anticyclone that forms in the Philippine Sea during a warm ENSO event.

The extent to which global air-sea interactions modify the *extratropical* ENSO teleconnections, on the other hand, is unclear. To date, the question has been addressed

[1] Workshop on Global Change in 20th Century and Seasonal and Interannual Climate Prediction. http://meop0.troja.mff.cuni.cz/workshop05/download/first_circular.pdf

only in a handful of modeling studies in which a GCM was forced by prescribed (observed or idealized) SSTs in the tropical Pacific and coupled to an oceanic mixed-layer model in the extratropics (Alexander 1992b, Bladé 1999) or globally (Lau and Nath 1996, 2001). The NH ENSO response in those coupled simulations was then compared to that in companion uncoupled simulations in which the mixed layer was replaced by climatological SSTs. The focus in all cases was on air-sea interactions in the North Pacific (even when the mixed layer extended to the entire oceanic domain) and the conclusions regarding the impact of this local midlatitude coupling on the upper tropospheric ENSO response ranged from weak damping to weak amplification (see Alexander et al. 2002 for a brief review). With the benefit of hindsight, however, it now seems evident that all those studies suffered from either low resolution (R15), insufficient sampling (4 ensembles), poor representation of the actual winter mixed-layer depth (50 m slab compared to observed ~100 m depths in the North Pacific), attribution problems (if the mixed layer was global) or several of the above.

Alexander et al. (2002, hereafter A02) revisited the issue by employing a medium resolution GCM (R30) and a full mixed-layer ocean model, increasing the ensemble size (8 to 16 experiments) and considering local coupling in the North Pacific separately from global coupling effects. Their experiments covered the period 1950-1999, which included 9 strong El Niño and La Niña events. The results revealed a modest but complex impact of air-sea interactions on the ENSO response in the North Pacific/North America (PNA) region: while global air-sea coupling (experiment MLM) weakly damped the signal in midwinter, air-sea interaction acting in isolation in the North Pacific (experiment NP-MLM) strongly amplified it in early spring. This effect resulted in unrealistically large

March anomalies and was mostly absent in the MLM experiment, suggesting that a crucial damping process originating in distant ocean basins was missing in the NP-MLM simulation. Indeed, an influence function diagnostic suggested that the weakening of the signal in the globally coupled experiment arose from a combination of stronger and partially canceling impacts from various remote oceanic areas (Indian Ocean, Atlantic Ocean, Kuroshio Current extension) superimposed on a weak local damping effect. The difficulties in attribution were compounded by the fact that the influence of coupling varied from month to month and by the large amount of spread between the monthly-mean ENSO composites of individual ensemble members. Thus, even an ensemble-size of 16 proved insufficient to ascertain the full impact of coupling on subseasonal timescales.

More important, Alexander et al. (2002) noticed that coupling induced changes in *tropical* precipitation in the Indo-Western Pacific region, *even when the mixed layer was confined north of 20ºN,* which could be an important factor in the modulation of the extratropical response. The potential role of tropical convection may explain some of the discrepancies between earlier studies. In particular, Lau and Nath (2001) found a strongly enhanced extratropical Niña signal in their globally coupled experiment, which they attributed to extratropical air/sea interactions; yet, a linear inverse modeling diagnosis of that experiment (Newman et al. 2000) suggested that extratropical coupling damped ENSO atmospheric anomalies over the central North Pacific. Likewise, Li et al. (2006) attribute changes in a GCM's response to tropical Pacific SST anomalies, upon incorporation of a mixed layer, to local extratropical coupling, but their mixed layer starts in the Tropics, extending northward from 10ºN.

This paper aims at clarifying the impact and origin of air-sea interactions on the NH

ENSO response. To improve on past results, the present study is based on a very large number (150) of simulations of the 1997/98 El Niño and 1998/99 La Niña events, following Sardeshmukh et al. (2000). This ensemble size enables us to assess coupling-induced variations not only in the mean signal, but also in the spread, and hence in the signal-to-noise ratio and predictability. Moreover, we can explore how coupling changes the probability distribution function (PDFs) of tropical convection and extratropical response, and the relationship between the two. Furthermore, in order to remedy past attribution problems and isolate the impact of the tropical western Pacific and Indian Oceans, we perform a set of separate experiments with coupling confined to these regions. We will show that coupling in the tropical northwest Pacific has the largest effect on the extratropical ENSO response, acting in such a way as to reinforce it, while the net effect of extratropical coupling is to weakly damp the response.

The paper is organized as follows. Section 2 contains a brief description of the model and experiments. Section 3 examines the SST anomalies induced by the atmospheric bridges. In section 4 we discuss changes in the extratropical and tropical ENSO response in response to coupling. The next section diagnoses the enhancement of the response in the tropically coupled experiment and explores the sensitivity to convection in the tropical northwest Pacific. Section 6 examines coupling-induced changes in the spread and predictability of the ENSO response. Summary remarks and a discussion of the results appear in section 7.

2. Description of model and experiments

In order to study the impact of air-sea coupling in various oceanic basins on the ENSO response, we conducted four sets of "super-ensemble" GCM simulations for the period

1996-99, using different oceanic configurations: NEUTRAL, CTRL, TROPMLM and MLM. In all but the NEUTRAL experiment, SSTs in the Tropical Eastern Pacific (15ºS-15ºN, 172º-South American coast) are prescribed to evolve according to observations (Figure 1). In the control (or CTRL) experiment, model "climatological" SSTs (see below) are specified at all oceanic grid-points[2] outside this region. In the MLM experiment, the atmosphere is coupled to a one-column entraining mixed-layer ocean model at each oceanic grid-point. In the TROPMLM experiment, this interactive ocean is restricted to the tropical Indian and western Pacific oceans (between 15ºS and 15ºN) and "climatological" SSTs are specified outside this region. Finally, in the NEUTRAL experiment, "climatological" SSTs are prescribed over the entire oceanic domain. Because of the absence of ocean currents, surface heat and salt flux corrections are required to maintain the oceanic seasonal cycle close to observations. Small biases in SST (<1°C), however, still occur in the long-term monthly means at a few locations after the corrections are applied. Thus the MLM experiment is performed first and its ensemble-mean 4-year-mean daily SSTs are used as the "climatological" SSTs in the remaining experiments. Although this ensures that all experiments share the same basic state and allows for a fair comparison, it has the disadvantage that the results cannot be cleanly contrasted with observations or longer GCM simulations. The experiments consist of 150 (100 in the TROPMLM case) realizations initiated from different atmospheric conditions taken from a different simulation. The characteristics of each experiment are summarized in Table 1.

The atmospheric model used is the GFDL R30 AGCM, which has an equivalent

[2] Oceanic grid-points at which ice is present at any time in winter are treated identically in all simulations: sea-ice (winter) or SST (summer), if applicable, is prescribed to repeat the observed climatological cycle. Hereafter "oceanic" refers to ice-free grid-points.

resolution of ~2.25º latitude by 3.75º longitude and 14 vertical sigma levels. For a description of the model and model's climate, the reader is referred to Gordon and Stern (1982), Broccoli and Manabe (1992) and Alexander and Scott (1995). The mixed layer model has been extensively documented in Alexander et al. (2000, 2002). It simulates mixed layer temperature (or SST), salinity and depth and includes local atmosphere-ocean fluxes, penetrating solar radiation and turbulent entrainment of water into the mixed layer.

Most results presented here are based on ensemble-mean monthly or seasonal mean anomalies, taken as deviations from the NEUTRAL ensemble-mean long-term mean (or "climatology"). At times, sub-ensemble means (referred to as "composites") are also computed. The statistical significance of the differences between means is assessed via a Student's t-test for unequal variances. For our large sample size, this method gives results that are virtually identical to those obtained using a Monte Carlo test such as that used in A02. For differences in spread and distribution, f-statistics and Kolmogorov-Smirnov (KS) tests are used. The 95% and 99% confidence levels are indicated in all plots.

This paper focuses on the NH ENSO response during the extended winter season (November to April). While the spatial pattern of the observed winter response is reasonably well reproduced by the GFDL model, the summer response is poorly simulated.

3. Oceanic response: the atmospheric bridges

We begin by examining the pattern of oceanic anomalies induced by the ENSO atmospheric bridges in the coupled experiments. Shown in Fig. 1 are two-month averages of SST anomalies during the Niño winter 1997/98 (hereafter ND, JF and MA refer to November-December, January-February and March-April) for runs MLM and

TROPMLM. The SST anomalies in the MLM experiment are very similar to those in the old MLM-16 (A02) simulations. The model reproduces the salient features of the observed global pattern (not shown), namely cold SST anomalies in the central north and south Pacific and warm SST anomalies in the subtropical/tropical Indian and Atlantic oceans. In the eastern hemisphere tropics, the SST anomalies are weak, on the order of a few tenths of a degree, and are indistinguishable from those in the TROPMLM experiment. In the western tropical Pacific, positive SST anomalies near the Equator gradually decay from their fall maximum, while cold SST anomalies develop between 10˚N-15˚N in late winter, both in qualitative agreement with observations (not shown). On the other hand, the bull's eye-like extension of the warm equatorial tongue east of 160˚E is likely an artifact of the sharp boundary at 172˚E between prescribed and predicted SSTs, combined with a small westward shift of the model's atmospheric response to ENSO relative to observations (A02). The simulated positive SST anomalies in the Indian Ocean are consistent with observations in ND but less so in JF, being weaker and less widespread, an unsurprising result considering both the absence of ocean dynamics and the fact that we are comparing a single observed event with a model ensemble.

4. Coupling-induced changes in the mean atmospheric response to ENSO

a) Extratropical circulation response

We now examine the differences between the coupled and uncoupled midlatitude flow responses to the 1997/99 ENSO events. The left panels in Fig. 2 show the evolution of the CTRL global upper tropospheric height response during the 1997/98 Niño winter. The middle and right panels display corresponding differences between the TROPMLM and CTRL and between the MLM and TROPMLM responses, respectively. The upper-level

circulation response is broadly similar in all three experiments: a pair of tropical anticyclones straddling the equator and centered around 150ºW, a wavetrain in the NH arching across the North Pacific and North America, peaking in JF, as well as the remains of the corresponding SH wavetrain propagating across the South Pacific (only visible in ND). Note that the NH response exhibits a more pronounced hemispheric-wide component in mid-winter than in early winter, both in the tropics and in the subtropics.

Even with these very large ensembles, there are few significant differences between the NH *extratropical* responses in the coupled and uncoupled experiments[3]. The most notable exception occurs in early winter (ND), when TROPMLM anomalies in the PNA region are stronger (~15%) and shifted about 30º westward relative to those in CTRL. This enhancement of the signal in early winter is equivalent barotropic and is more manifest at lower levels: the ND TROPMLM−CTRL differences at 500 hPa, 850 hPa and at sea level at the center of the North Pacific anomaly are ~ 20%, 25% and 30%, respectively (not shown). In mid-winter (JF), the differences are very small. The ND MLM−TROPMLM differences are much weaker, indicating that coupling to the remaining oceans does not significantly modify the response, i.e., most of the changes in the MLM response relative to CTRL are due to tropical coupling. Corresponding results for the La Niña event are qualitatively similar, but the enhancement of the coupled signal is most pronounced in midwinter, particularly in TROPMLM (~20%, not shown, but see Fig.3). However, because the signal-to-noise ratio is much weaker for the La Niña event, the coupling-induced differences are not statistically significant.

[3] The small but significant differences in the tropics reflect a strengthening/lingering of the zonal mean ENSO response in the coupled experiments, which is due to the lagged warming of the tropical Indian and Atlantic oceans (Fig. 1), as has been discussed by Kumar and Hoerling (2003).

The differences in the Niño/Niña height response over the North Pacific can be better appreciated in Fig. 3a, which displays the evolution of the 30-day running-mean 500-hPa height anomalies averaged over 32ºN-48ºN and 176ºE-135ºW (see box in Fig. 2). Clearly, the response is stronger in TROPMLM than in CTRL for most of the Niño winter and all of the Niña winter. This enhancement is statistically significant at the 95% level over the course of each winter (i.e., seasonal means), although on a 30-day basis it is only significant during early winter and (briefly) during late winter of the Niño event. Because the coupling-induced differences are roughly linear with respect to the phase of ENSO, the NIÑO−NIÑA (warm−cold) TROPMLM anomaly (Fig. 3b) is also stronger than the CTRL one throughout the entire winter, from November to March, but again these differences do not pass the 95% significance test in mid winter.

The North Pacific MLM warm – cold anomaly is also significantly stronger than the CTRL one in early winter, but it is damped relative to TROPMLM in mid-winter, suggesting that global coupling acts to cancel out the enhancement due to tropical coupling in the tropical western Pacific and Indian oceans. Although not significant, this result is consistent with the earlier findings of A02. The similar evolution of the height anomalies during the decay phase in all three experiments suggests that midlatitude "reduced thermal damping" (Bladé 1997, Barsugli and Battisti 1998) does not play a critical role in enhancing the persistence of atmospheric anomalies.

b) Tropical precipitation response

The differences between the TROPMLM and CTRL extratropical responses presumably arise from changes in the tropical heating field in the presence of interactive western Pacific and Indian oceans. The CTRL tropical rainfall anomalies during the Niño and Niña winters

are shown in Fig. 4, together with the TROPMLM – CTRL difference fields. The Niño precipitation response is characterized by an equatorial dipolar pattern with positive anomalies at and east of the dateline and weaker negative anomalies to the west. Its evolution follows the seasonal march of convection (not shown): as winter progresses, the region of enhanced convection shifts southward and expands towards the south central tropical Pacific, while the suppressed precipitation peaks and moves northward. The Niña anomalies are similar and opposite, but weaker and shifted 30º west.

Consistent with the extratropical height changes, the largest tropical precipitation differences in TROPMLM relative to CTRL occur in ND-97 when a patch of anomalous equatorial convection is found near the nodal line of the dipole (~ 160ºE), i.e., over the warm, interactive, western Pacific ocean. This change results in a small westward shift of the dipolar pattern, so that weakly reduced precipitation near 160ºE is replaced by weakly enhanced precipitation. A similar but opposite (and weaker) anomaly pattern is found in ND of the Niña winter, persisting into JF. Instead, in midwinter of the Niño winter, TROPMLM − CTRL differences in the rainfall response are small and occur south of the Equator.

The precipitation anomalies in MLM are almost indistinguishable from those in TROPMLM. This result, along with the previously discussed differences in the CTRL, TROPMLM and MLM height responses, suggests that the impact of global air-sea coupling upon the extratropical ENSO response is comprised of two parts, an amplification due to tropical coupling and a damping due to extratropical coupling. Analysis with influence functions suggests that this midwinter damping may itself involve a combination of mechanisms and remote forcings from different oceanic basins (not shown, but see A02). In the remainder of this paper, however, we will focus upon the

other portion of the coupled signal, the amplification due to tropical coupling.

5. Enhancement of the extratropical ENSO response due to tropical coupling

In this section, we investigate the enhancement of the extratropical ENSO response in experiment TROPMLM, focusing on December 1997, when this effect is most significant (Fig. 3a). The CTRL upper-level height and tropical precipitation anomalies for this month (Figs. 5a-c) and the corresponding TROPMLM−CTRL difference fields (Figs. 5b-d) are strongly suggestive of a relationship between enhanced extratropical response and increased tropical rainfall near 160ºE. To further explore the sensitivity of North Pacific heights to tropical northwest Pacific convection, we will define indices of tropical convection and extratropical response by computing weighted averages of total precipitation and 200-hPa height anomalies over specified regions.

a) Quartile compositing:

We first stratify the TROPMLM ensemble according to an index of precipitation averaged over the region of significant (>0.05 cm/day) TROPMLM − CTRL mean December 1997 differences (see Fig. 5d). Upper and lower quartile composites (sub-ensembles) constructed by averaging the precipitation over either the entire region or the southern portion of that region did not produce markedly different extratropical responses (not shown). On the other hand, corresponding composites based on precipitation averaged over the *northern portion* of that region (north of 3ºN, see purple line in Fig. 5d) exhibit very pronounced and significant differences in the amplitude and structure of the extratropical upper-level height anomalies (Fig. 6e-f), with even stronger differences at lower levels (not shown). Hereafter, this off-equatorial region will be referred to as the

TNWP (tropical northwest Pacific) region. Note that each of these quartile composites comprises 25 members.

The TNWP region of anomalous precipitation is now clearly visible in the upper quartile composite of both anomalous and total precipitation (Figs. 6b-6d) as a tail of convection extending northwestward from the dateline to 20ºN, or, equivalently, as a delay in the seasonal southward migration of convection in this area. This is also evident in Fig. 7a, which shows that the precipitation pattern in the upper−lower quartile composite is characterized by a meridional dipole, with enhanced (decreased) rainfall north (south) of the Equator. The associated anomalous diabatic heating (not shown) appears to generate a secondary Rossby wavetrain (Fig 7d) that is superimposed upon the main wavetrain emanating from the central equatorial Pacific (Figs. 2-5a) and interferes constructively with it over the PNA region, leading to the enhanced height response in the upper quartile composite (Fig. 6f). This secondary wavetrain also deepens the surface low in the northeast Pacific (Fig. 7e) and results in enhanced precipitation along the northwest coast of the US (Fig. 6d). The low pressure anomaly in the TNWP region is significant at the 99% level and the only large-scale feature in the entire tropics (Fig. 7e). Also shown in Fig. 7 are corresponding upper-lower quartile differences in SST and surface specific humidity. The specific humidity field indicates enhanced humidity in the TNWP region in the upper quartile composite, possibly due to enhanced low-level moisture convergence associated with the anomalous surface low. In contrast, corresponding SST differences are weak and non-local (Fig. 7b).

b) Influence of TNWP convection on the extratropical ENSO response:

The quartile analysis indicates a substantial influence of TNWP convection on the

extratropical ENSO wavetrain and supports the notion that the early winter enhancement of the ensemble-mean TROPMLM (and MLM) extratropical response is due to convective anomalies that tend to develop in the TNWP region in the presence of coupling. Furthermore, there are several indications that convection in this relatively confined off-equatorial region of the tropical northwest Pacific is just as effective at forcing circulation anomalies in the PNA region, *or more so*, than large-scale convection in the central equatorial Pacific (CEP), at least in early winter. First, the relative magnitudes of the height response and rainfall anomaly are comparable for the primary and secondary wavetrains (Figs. 5a-c and 7a-d), but in the latter the convective forcing is concentrated over a smaller area. Additionally, even though precipitation variability is much stronger in the CEP than in the TNWP region, TROPMLM upper/lower quartile composites based on an index of CEP precipitation (as defined by the 0.5 cm/day contour in Fig. 5c) do not produce significantly different extratropical responses (not shown), suggesting that the December ENSO response is actually more sensitive to TNWP convective anomalies. At the same time, compositing or regressing the precipitation field against the North Pacific 200-hPa height anomaly (as defined by the region within the -60 m contour in Fig. 5a) returns a pattern characterized by stronger convection in the TNWP than in the CEP region. Indeed, the correlation between the strength of this North Pacific low and TNWP convection is 99% significant (-0.26), unlike the correlation with the CEP precipitation index (-0.12). Moreover, if we define a North Pacific *wavetrain* index as the difference between the (area-averaged) anomalies in the northeast Pacific and western Pacific centers of action (Fig. 7d), then the correlation between TNWP convection and North Pacific response increases to -0.51, as shown in the scatter plot in Fig. 8.

c) Coupling-induced changes in TNWP convection:

Given that convection in the TNWP region appears to strongly influence the ENSO extratropical response in early winter of the Niño year, we now explore the influence of air-sea coupling on this forcing mechanism. In particular, we need to address the following questions: how does coupling in the western Pacific change the forcing (that is, TNWP convection) and does it also change the extratropical sensitivity to that forcing? Additionally, why is this phenomenon limited to early winter?

Figure 9, which compares the PDF of December 1997 and January 1998 TNWP precipitation in the two experiments, confirms the impression from Figs. 4b-d and 5d that coupling significantly affects convection in the TNWP region in December but not in January. Moreover, the December changes are not linear: the TROPMLM PDF (or histogram) is not merely shifted towards heavier mean precipitation relative to CTRL, but has increased variance and is more strongly skewed towards positive values. In fact, ND precipitation variability in the TNWP region increases significantly at all times scales, from daily to seasonal, and particularly at intraseasonal timescales (Fig. 10b), whereas corresponding JF changes are much weaker and located south of the Equator (Fig. 10d). Incidentally, the spatial pattern of the coupling-induced changes in intraseasonal variability is similar to that of the corresponding changes in monthly-mean precipitation (cf. Figs. 4b (4d) with Fig. 10b (10d)]. Note that the same correspondence exists between *Niño-induced* anomalies in mean precipitation and in precipitation variability [cf. Fig. 4a (4c) with Fig. 10a (10c)], a result earlier obtained by Compo et al. (2001).

The coupling-induced shift in the distribution of December TNWP precipitation is also evident in the scatter plot of Fig. 8. Note that the relationship between TNWP convection

and Z-200 anomalies is similar in CTRL and TROPMLM, with a correlation of about 0.5. To first order then, the effect of coupling is not to change the sensitivity of North Pacific heights to the forcing, but to shift the distribution of TNWP convection towards higher values, which results in a shift of the Z-200 distribution towards higher (negative) values and hence a stronger ensemble-mean response (see thick dot and plus marks in Fig. 8). At the same time, despite the increase in TNWP variance, the Z-200 variance is decreased (not shown, but see Fig. 3c), which could occur if there were a saturation of the height response at high forcing (larger positive precipitation anomalies). The quadratic fit (dashed line) in Fig. 8 is suggestive of such a weakly nonlinear relationship, but it cannot pass an F-test to distinguish it from the linear fit (solid line).

So, why does coupling enhance TNWP convection in early fall? In early winter, the monthly-mean SST in the tropical western Pacific is only ~0.5ºC warmer in TROPMLM than in CTRL (Fig. 1), but these SST anomalies occur relative to a very warm base state (Fig. 11). The TNWP region, in particular, lies at the northern edge of the western Pacific warm pool and over water climatologically warmer than 28ºC — the threshold value for deep convection in observations (Graham and Barnett 1987) and in the model (not shown). One might then *qualitatively* expect the precipitation to be very sensitive to even modest positive SST departures, simply by virtue of the nonlinear increase in evaporation that follows from the Clausius-Clapeyron relationship (a 0.1% increase in SST implies a 2% increase in saturated specific humidity). Enhanced evaporation, low-level humidity and moisture convergence in the tropical western Pacific indeed occur in the TROPMLM experiment (Figs. 5f , 5h and 5j), together with a weaker increase in sensible heat flux and surface air temperature (Figs. 5e and 5g). This low-level warming should help reduce

the surface pressure hydrostatically (Lindzen and Nigam 1987) and lead to a strengthening of the surface circulation and moisture flux convergence (Figs. 5i-5j). In this way, the warm (mean) SST anomalies that develop in the western tropical Pacific in early fall in the coupled experiments (Fig. 1) could favor the development and/or intensification of TNWP tropical convective disturbances later in the season.

Of course, non-local mean and anomalous SST effects cannot be ruled out. For instance, there may be some weak feedback imparted by the small but statistically significant SST anomalies in Fig. 7b. Indeed, an index constructed using SST anomalies in the TNWP region minus SST anomalies west of New Guinea is correlated with TNWP precipitation at 0.37 (December 1997). Overall, however, the TROPMLM increase in TNWP precipitation (in both the mean and variance) need only be due to the mean SST change.

d) Impact of the annual cycle on the sensitivity of the North Pacific circulation to TNWP forcing:

Next, we test whether the TNWP region is always effective at forcing flow anomalies over the PNA region. Application of the quartile composite analysis to other winter months/years and other experiments shows that, regardless of SST conditions, convection in the TNWP region tends to generate a strong low over the North Pacific throughout winter (November through February). This is true even for Niña years and for the NEUTRAL experiment. The only exception appears to be during mid-winter of the Niño year, when the sensitivity of North Pacific heights to anomalous convective heating in the TNWP region vanishes. To illustrate this finding, Fig. 12 shows CTRL precipitation and Z_{200} upper − lower quartile composite differences for December, January and February of a non-ENSO winter (1996/1997) and of the Niño winter (1997/98), again based on the TNWP precipitation index. For the non-ENSO winter, convection in the TNWP region

excites a pattern of extratropical height anomalies very similar to that in Fig. 7d in all months (although in February 1997 the source region of the wavetrain is less distinct). This wavetrain is also present in December of the Niño winter but is mostly absent in January and totally absent in February 1998. In January, one can still see a response to TNWP heating, but it is more zonally symmetric and appears trapped in the subtropics.

This change in the "teleconnectivity" of the TNWP region appears related to subtle ENSO-induced variations in the basic state rather than to differences in the tropical forcing, since the amplitude and extent of the TNWP precipitation anomalies is comparable in all six cases in Fig. 12. The existence of an optimal forcing region in the TNWP region for circulation anomalies in the PNA sector was first suggested by Simmons et al. (1983). Hamilton (1988) also found that observed wintertime seasonal ENSO anomalies are more highly correlated with SSTs in the Indo-Western Pacific region than with SSTs in the central/eastern equatorial Pacific, with the extratropical response being most pronounced when the far western Pacific is anomalously warm. Newman and Sardeshmukh (1998) showed that sensitivity of North Pacific circulation anomalies to Rossby wave forcing over the western tropical Pacific is potentially much greater in late fall than in mid-winter, whereas the opposite is true for forcing over the central Pacific. This is a result of a stronger Pacific jet in midwinter and an associated waveguide that steers Rossby waves generated in the TNWP region initially northeastward but then southeastward into the eastern tropical Pacific, effectively tropically trapping the disturbances. Instead, during late fall (and again in spring) the jet is relatively weaker and guides waves generated in the TNWP region across the Pacific and over into North America. Newman and Sardeshmukh also suggested that the GFDL-R30 model used in

the current study might be relatively too sensitive to forcing in the western tropical Pacific in mid-winter, owing to a simulated climatological jet that is somewhat weaker and farther poleward than in nature (Alexander and Scott 1995) and thus fails to reproduce the observed wave trapping effect. In midwinter of a Niño year, however, the simulated jet is stronger (not shown), so that the expected seasonal shift of sensitivity from the western to the central Pacific can then occur from December to January. This effect can explain the lack of an extratropical response to TNWP anomalies in January/February 1998 (Fig. 12).

e) Midwinter response and insensitivity to tropical coupling:

A remaining question concerns why neither TNWP convection nor the ENSO response are impacted by the presence of coupling in midwinter of the Niño year. In January the climatological 28ºC isotherm in the tropical northwest Pacific retreats south, from 15ºN to 10ºN, and SSTs in the TNWP region decrease between 0.5 and 1ºC (Fig. 11). The coupled SST anomalies are also weaker (Fig. 1). More important, the main area of ENSO-induced convection in the central equatorial Pacific is displaced south (Fig. 4c), and mean precipitation in the TNWP region is strongly suppressed. The positive convective anomalies induced by coupling (Fig. 4d) shrink and no longer occur over the TNWP region, whose teleconnectivity to the North Pacific is blocked due to changes in the background state. Given this conjunction of adverse factors, it is not surprising that the mid-winter extratropical response to ENSO does not appear to feel the presence of coupling.

Now, recall that the enhancement of the coupled extratropical response during *La Niña*, although not statistically significant, actually peaks in midwinter (Fig. 3a). As one would expect, significant changes in TNWP convection (stronger negative anomalies) are seen at that time (Fig. 4f-h). This is also in keeping with our earlier discussion, in the sense that, in

the model, the sensitivity of PNA anomalies to TNWP convection should persist into midwinter unless the jet becomes much stronger (as occurs during Niño). That the impact of coupling on TNWP convection should be nonlinear relative to the phase of ENSO is also not surprising, since the convective response to ENSO is itself asymmetric (cf. Fig. 4c and 4g) and the evaporation-SST feedback is nonlinear and depends on the absolute SST. This result also suggests that the enhancement of the early winter extratropical Niño response is not critically due to the bull's eye in SST, since no such feature exists during La Niña, only a weak but widespread cooling in the western tropical Pacific (not shown).

Returning to the change in teleconnectivity from December to January (Fig. 12) of a Niño winter, it is worth pointing out that the transition in the character of the TNWP-forced wavetrain is reminiscent of the changes in the mean ENSO response from early to mid-winter (Fig. 2). As we noted, this response exhibits a more pronounced hemispheric wide component in the core of winter, at the time when the negative convective anomaly peaks in amplitude and moves to the TNWP region (Fig. 4c). This anomaly is maximized in the *lower* quartile composite for January 1998 and inspection of the corresponding height response (not shown) reveals stronger negative anomalies over southeastern Asia and the southeastern US compared to the upper composite or the mean pattern in Fig. 2, which account for the positive zonally symmetric subtropical features in Fig. 12d. Hence, in the same TNWP region in which anomalous convection in early winter favors the development of a stronger ENSO teleconnection, suppressed convection in midwinter confers a more hemispheric wide, zonally symmetric, subtropical component to the ENSO response.

6. Coupling-induced changes in the spread of the atmospheric response to ENSO

To conclude, we examine changes in the spread of the extratropical ENSO anomalies

in response to tropical and global coupling. It is readily apparent from Fig. 3c, which depicts the evolution of the standard deviation (std) of the 30-day running-mean 500-mb height response averaged over the North Pacific, that the impact of *tropical* coupling is to systematically reduce the spread of the response. Figure 3c also shows that the incorporation of coupling in the remaining oceans (run MLM) restores the "noise" of the response back to its original CTRL level. Although the decrease in spread in TROPMLM is not statistically significant on this 30-day time scale, it is discernible throughout the entire warm and cold ENSO cycles and is very significant in winter 1998 for longer two-monthly JF or seasonal JFM means (Fig. 13, middle panels). Because the JFM mean signal is also slightly stronger (Fig 13, top panels), the signal-to-noise ratio, or predictability, of the ENSO response increases throughout the central North Pacific in the TROPMLM experiment, by up to 50% (Fig. 13, bottom panels).

The TROPMLM−CTRL differences in the standard deviation of JFM precipitation do not reveal a corresponding reduction in the spread of the forcing (not shown) and are thus not suggestive of a link between tropical noise and extratropical noise. We then computed the PDF of the circulation response in the North Pacific and inspected the actual distribution changes associated with the decrease in spread. The inset in Fig. 13 shows the PDFs of JFM 500-mb heights averaged over the region of maximum reduction in spread (37ºN-50ºN, 150ºE-150ºW). The two sampled distributions differ significantly at the 95% level, as measured by the KS goodness-of-fit test (Kendall and Stuart 1997), as well as in means and standard deviation (99% level). It is clear, however, that the higher predictability of the TROPMLM response is mainly due to a reduced positive skewness and non-gaussianity, i.e. decreased frequency of anomalous ridging over the central

North Pacific during the El Niño event (24 realizations in CTRL versus 6 in TROPMLM). Thus the impact of tropical coupling is more complex than a simple linear reduction in the spread of the signal. This effect is not observed in early winter and thus appears unrelated to the previously discussed TNWP effect.

7. Conclusions

a) Summary

We have analyzed the impact of tropical and global coupling on the extratropical NH winter ENSO teleconnection by means of "super-ensembles" of coupled and uncoupled simulations of the 97/98 El Niño and 98/99 La Niña events. The results indicate that air/sea interactions in the tropical Indo-western Pacific ocean amplify the ENSO response in the PNA region, except in midwinter of the Niño year. This enhancement is most pronounced in early winter of the Niño year and is chiefly due to increased convection (subsidence) in a small area of the tropical northwest Pacific (which we refer to as the TNWP region) during El Niño (La Niña), as can be verified by stratifying the individual responses according to an index of precipitation in this region (quartile compositing). This effect is also evident in the globally MLM coupled experiment, but Figs. 3a-b suggest that *global* coupling tends to counteract the influence of tropical coupling.

Further analysis shows that, in this model, the TNWP region constitutes an "optimal" forcing region for PNA circulation anomalies throughout the winter season, irrespective of the presence of coupling or SST conditions in the tropical Pacific. The exception appears to be the core of winter of an El Niño year, when the teleconnection from the TNWP region is trapped in the subtropics. At any other time and, in particular, early in the Niño winter, anomalous convection in the TNWP region excites a wavetrain that

interferes constructively with the main ENSO wavetrain emanating from the central equatorial Pacific. Because the PDF of TNWP convection is shifted towards higher values in the presence of coupling, so is the PDF of the extratropical response to this forcing; thus, the ENSO teleconnection is amplified.

We suggest that the intensification of the TROPMLM convection (in both the mean and the variance) in the TNWP region in early winter occurs (at least partly) via increased evaporation associated with a slightly warmer western Pacific — a residual coupling effect from the previous fall. In the presence of such a warm basic state (SST >28ºC), even modest coupled SST anomalies can result in large changes in convection, either by triggering more disturbances or by amplifying the naturally occurring ones. Although this effect is modest, it has a very large impact on the early winter extratropical Niño response because of its high sensitivity to forcing from the TNWP region. The insensitivity of the midwinter Niño teleconnection to coupling may then be due both to colder mean SSTs and to the suppressed teleconnectivity between the PNA and TNWP regions; the latter is consistent with ENSO-induced changes in the basic state and implied changes in the Rossby waveguide.

Tropical coupling also leads to increased predictability of the seasonal mean JFM ENSO signal over a large portion of the North Pacific, but again this effect is offset in MLM. Dissecting the weak damping in the MLM experiment poses a challenge as it appears to result from a combination of stronger, partially canceling, impacts from different oceanic basins. The important result is that most of the impact of global coupling on the ENSO response appears to actually originate in the tropics.

b) Discussion:

As discussed, for example, by DeWeaver and Nigam (2004), the "protomodel" for

ENSO teleconnections remains one of a single Rossby wavetrain emanating from a wide region of anomalous convection in the central equatorial Pacific (CEP). Yet, numerous studies have shown that there are in fact multiple SST and heat sources/sinks across the tropics and subtropics during ENSO, which contribute to the observed extratropical response. For example, Barsugli and Sardeshmukh (2002) suggest that tropical Pacific SST anomalies west of the date line are very effective at exciting the PNA pattern. The Rossby wave response to anomalous Indian Ocean heating during ENSO events tends to oppose the response to tropical Pacific SST anomalies over the PNA region (Ting and Sardeshmukh 1993; A02; Annamalai et al. 2006). Indonesian cooling plays an important role in Branstator (1985) and Ting and Hoerling (1993) simulations, while DeWeaver and Nigam (2004) emphasize that the *observed* regions of diabatic cooling that surround the central heating region are just as important in forcing ENSO teleconnections. Thus, convective anomalies in the Indo-Western Pacific sector and their modulation by interactions with the ocean appear critical for a complete understanding and prediction of the extratropical response to ENSO.

The present work contributes further insight into the forcing of ENSO teleconnections by suggesting the existence of a "hot button" convective region in the tropical northwest Pacific, to which flow anomalies in the PNA sector are very sensitive, and which can significantly influence the direct response to CEP heating. Moreover, most of the impact of air/sea interactions on the ENSO teleconnection in the TROPMLM, and also in the MLM, experiment appears to originate from changes in the convection in this TNWP region. This result confirms the impression from A02 that *tropical* coupling may be the most important factor in modulating the ENSO response and possibly extratropical

variability in general. It also cautions against precipitously attributing midlatitude coupled-uncoupled differences to local air/sea feedbacks when the mixed layer extends into the Tropics. For instance, Li et al. (2006) assert that extratropical air/sea interactions cause the enhancement of the coupled midlatitude response to tropical west Pacific SST anomalies in their GCM simulations, but their mixed layer extends to the entire NH northward of 10ºN, so their result could involve coupling-induced changes in tropical convection.

As discussed in section 5d, simple arguments involving Rossby wave propagation on the observed basic state support the existence of an "optimal" forcing region in the tropical northwest Pacific for PNA circulation anomalies in early winter (and not in midwinter). Furthermore, observational support for this notion can be drawn from regressions of SST and precipitation against the North Pacific index — a measure of the strength of the Aleutian low (Trenberth and Hurrell 1994). Figure 14 shows such regressions computed separately for December and January monthly-mean data for the period 1950-1999. There is considerably more North Pacific sensitivity to TNWP SST and precipitation anomalies in December than in January, with the converse holding true for anomalies in the central tropical Pacific, much as occurs in the model during a Niño year, and consistent with our waveguide reasoning (Section 5d). Note also the strong similarity between the observed and simulated December precipitation patterns (Fig. 7a). Because of a relatively weak simulated jet, in the model the teleconnectivity between the TNWP and PNA regions is present throughout most of the winter in non-ENSO or Niña years, and only vanishes in midwinter during a Niño event, when the jet is stronger. In this case, the suppressed convection that occupies the TNWP region at this time appears to reinforce the hemispheric-wide, longitudinally symmetric, component of the ENSO

teleconnection. Interestingly, the observed ENSO signal displays some similar features, with an amplification of the wave 0-3 stationary pattern during some strong Niño events in January (K. Weickmann, personal communication). All in all, it is clear that how coupling affects convection in the TNWP region may well play an important role in determining the winter response to ENSO.

Although not emphasized in this paper, we also find another early to mid-winter change in the character of the ENSO teleconnection. In mid-winter, the ENSO response tends to be rather insensitive to the strength of CEP convection, in contrast with the early winter response, which shows a more linear relationship between the two. For instance, if we stratify the CTRL geopotential height field according to an index of CEP precipitation and compare upper and lower quartile composites, we find that in December 1997 the strength of both CEP convection and North Pacific low is double in the upper composite (Fig 15, top panels). Instead, in January 1998, a 60% difference in the strength of CEP convection has no bearing on the amplitude of this North Pacific response (Fig. 15, bottom panels). The finding may be interpreted as consistent with recent modeling results of Sardeshmukh and Compo (personal communication), which indicate that the North Pacific winter response to CEP SST anomalies is saturated at high values of SST forcing.

There are some important caveats to this study. First, the simulated SST anomalies are generally weak. In midlatitudes this is due, in part, to the lack of Ekman currents, but experiments analogous to the MLM-16 runs discussed in A02, with the additional incorporation of Ekman transport, indicate that the additional feedback on the atmospheric circulation is minimal. Coupling with the Indian Ocean, however, may be critically dependent on the presence of oceanic Rossby waves and so may not be properly

captured in any of our simulations. The impact of coupling on the TNWP region may also be somewhat related to the sharp boundary (no blending) between prescribed and predicted SST. Finally, as noted earlier, the sensitivity to TNWP forcing could be overestimated in the model due to biases in its basic state.

Finally, from the point of view of interannual predictability there are two important points worth making. One is that these results serve to emphasize Newman and Sardeshmukh's (1998) finding that the sensitivity of the PNA region to SST/convective forcing (and, implicitly, air/sea coupling) in the Indian and Pacific Ocean can vary substantially from month to month. The other is that the decision on where to set the boundary between prescribed and predicted SST in partially-coupled ("pacemaker") experiments should take into account the potential role of the TNWP as an important forcing region for PNA circulation anomalies. Future work is planned in order to generalize the present results to other GCMs. It will be interesting to see if the coincidental nature of the TNWP as a region both highly teleconnected to the North Pacific and highly "reactive" to the presence of coupling (and the simultaneous disappearance of both characteristics at certain times) can be replicated in other GCMs.

Acknowledgments: We are very grateful to John Young and Brian Mapes whose comments, suggestions and enthusiasm provided a big motivation for this study and greatly improved the manuscript. Gil Compo and Prashant Sardeshmukh also made helpful comments. We also thank Jon Escheid for supplying the gridded GHCN precipitation data. IB is a researcher supported by the Ramón y Cajal Program, funded by the Spanish MCYT.

References

Alexander, M. A., 1992a: Midlatitude atmosphere-ocean interaction during El Niño. Part I: the North Pacific Ocean. *J. Climate*, **5**, 944-958.

Alexander, M. A., 1992b: Midlatitude atmosphere-ocean interaction during El Niño. Part II: the north hemisphere atmosphere. *J. Climate*, **5**, 959-972.

Alexander, M. A,. and J. D. Scott, 1995: Atlas of climatology and variability in the GFDL R30S14 GCM. CIRES, Univ. of Colorado, 121 pp. [Available from the authors at CDC/NOAA, R/CDC1, 325 Broadway, Boulder, CO. 80305-3328].

Alexander, M. A., J. D. Scott, and C. Deser, 2000: Processes that influence sea surface temperature and ocean mixed layer depth variability in a coupled model. *J. Geophys. Res*., **105**, 16,823-16,842.

Alexander, M. A., I. Bladé, M. Newman, J. R. Lanzante, N.-C. Lau, and J. D. Scott, 2002: The atmospheric bridge: the influence of ENSO teleconnections on air-sea interaction over the global oceans. J. Climate , 15, 2205-2231

Alexander, M. A. and J. D. Scott, 2002: The influence of ENSO on air-sea interaction in the Atlantic. *Geophys. Res. Lett*., **29(14)**, 10.1029/2001GL014347.

Annamalai, H., H. Okajima, and M. Watanabe, 2006: Possible Impact of the Indian Ocean SST on the Northern Hemisphere Circulation during El Nino. *J. Climate*, in press.

Barsugli, J. J., and P. D. Sardeshmukh, 2002: Global atmospheric sensitivity to tropical SST anomalies throughout the Indo-Pacific Basin. *J. Climate,* **15,** 3427-3442.

Barsugli, J. J., and D. S. Battisti, 1998. Basic Effects of Atmosphere-Ocean Thermal Coupling on Midlatitude Variability. *J. Atmos. Sci*., **55**, 477-493.

Bladé, I., 1997: The influence of midlatitude ocean-atmosphere coupling on the low-frequency variability of a GCM. Part I: No tropical SST forcing. *J. Climate*, **10**, 2087-2106.

Bladé, I., 1999: The influence of midlatitude ocean-atmosphere coupling on the low-frequency variability of a GCM. Part II: Interannual variability induced by tropical SST forcing. *J. Climate*, **12**, 21-45.

Branstator, G., 1985: Analysis of General Circulation Model Sea-Surface Temperature Anomaly Simulations Using a Linear Model. Part I: Forced Solutions. *J. Atmos. Sci*., **42**, 2225-2241.

Broccoli, A. J., and S. Manabe, 1992: The effects of orography on midlatitude Northern Hemisphere dry climates. *J. Climate*, **5**, 1181-1201.

DeWeaver, E., and S. Nigam, 2004: On the forcing of ENSO teleconnections by anomalous heating and cooling. *J. Climate*, **17**, 3225-3235.

Graham, N. E., and T. P. Barnett, 1987: Sea surface temperature, surface wind divergence and convection over tropical oceans. *Science*, **238**, 657-659

Gordon, C. T., and W. F. Stern, 1982: A description of the GFDL global spectral model. *Mon. Wea. Rev*., **110**, 625-644.

Hamilton, K., 1988: A detailed examination of the extratropical response to tropical El Niño/Southern Oscillation events. *J. Climatol.*, **8**, 67-86.

Huang, H.-P., R. Seager and Y. Kushnir, 2005: The 1976/77 transition in precipitation

over the Americas and the influence of tropical SST. *Clim. Dyn*., **24**, 721-740.

Kendall, M., and A. Stuart, 1977: The Advanced Theory of Statistics. 3d ed. Vol. 1. Macmillan, 283 pp.

Krishna Kumar, K.**,** M. Hoerling**,** and B. Rajagopalan, 2005: Advancing dynamical prediction of Indian monsoon rainfall. *Geophys. Res. Lett.*, **32**(8), L08704, 10.1029/2004GL021979, 4 pp.

Kumar, A., and M. P. Hoerling, 1998: On the specification of regional SSTs in AGCM simulations. *J. Geophy. Res*., **103**, 8901-8907.

Kumar, A., and M. P. Hoerling, 2003: The nature and causes for the delayed atmospheric response to El Niño. *J. Climate*, **16**, 1391-1403.

Lau, N.-C., and M. J. Nath, 1996: The role of the 'atmospheric bridge' in linking tropical Pacific ENSO events to extratropical SST anomalies. *J. Climate*, **9**, 2036-2057.

Lau, N.-C., and M. J. Nath, 2000: Impact of ENSO on the Variability of the Asian-Australian Monsoons as Simulated in GCM Experiments. *J. Climate*, **13**, 4287-4309.

Lau, N.-C., and M. J. Nath, 2001: Impact of ENSO on SST variability in the North Pacific and North Atlantic: seasonal dependence and role of extratropical air-sea coupling. *J. Climate*, 14, 2846-2866.

Li S., M. P. Hoerling, S. Peng, and K. M. Weickmann. 2006: The Annular Response to Tropical Pacific SST Forcing. *J. Climate*, **19**, 1802-1819.

Lindzen, R.S., and S. Nigam, 1987: On the role of sea surface temperature gradients in forcing low-level winds and convergence in the tropics. *J. Atmos. Sci*., **44**, 2418-

2436.

Luksch, U., and H. v. Storch, 1992: Modeling the low-frequency sea surface temperature variability in the North Pacific. *J. Climate*, **5**, 893-906.

Newman, M., and P. D. Sardeshmukh, 1998: The impact of the annual cycle on the North Pacific/North American response to remote low frequency forcing. *J. Atmos. Sci.*, **55**, 1336-1353.

Newman, M., M. A. Alexander, C. R. Winkler, J. D. Scott, and J. J. Barsugli, 2000: A linear diagnosis of the coupled extratropical Ocean-Atmosphere system in the GFDL GCM. *Atmospheric Sciences Letters*, **1**, 14-25.

Palmer, T. N. And Coauthors, 2004: Development of a European multi-model ensemble system for seasonal to inter-annual prediction (DEMETER). *Bull. Amer. Met. Soc,* **85**, 853-872.

Reynolds, R. W. and T. M. Smith, 1994: Improved global sea surface temperature analyses using optimum interpolation. *J. Climate,* **7**, 929-948.

Sardeshmukh, P. D., G. P. Compo, and C. Penland, 2000: Changes of probability associated with El Niño. *J. Climate*, **13**, 4268-4286.

Simmons, A. J., J. M. Wallace, and G. W. Branstator, 1983: Barotropic Wave Propagation and Instability, and Atmospheric Teleconnection Patterns. *J. Atmos. Sci.*, , **40**, 1363-1392.

Seager, R., 2006: The Turn of the Century drought across North America: global context, dynamics and past analogues. *J. Climate*, submitted.

Ting, M. F. and P. D. Sardeshmukh, 1993: Factors Determining the Extratropical

Response to Equatorial Diabatic Heating Anomalies. *Journal of the Atmospheric Sciences*, **50**, 907-918.

Ting, M., and M. P. Hoerling, 1993: Dynamics of stationary wave anomalies during the 1986/87 El Niño, *Climate Dynamics*, **9**, 147-164.

Trenberth, K.E. and J.W. Hurrell, 1994: Decadal Atmosphere-Ocean Variations in the Pacific. *Climate Dynamics*, **9**, 303-319.

Wang, B., R. Wu, and X. Fu, 2000: Pacific East-Asian teleconnection: How does ENSO affect east Asian climate. *J. Climate,* **13**, 1517-1536.

Wang, B., X. Fu, Q. Ding, I.-S. Kang, K. Jin, J. Shukla and F. Doblas Reyes: Challenges in prediction of the summer monsoon rainfall: inadequacy of the two-tier strategy (submitted to J. Climate).

FIGURES

FIGURE 1. Two-month means of winter SST anomalies in the MLM (left) and TROPMLM (right) experiments for the 1997/98 NIÑO event. Contour interval is 0.2 ºC. The box in the middle right panel denotes the region of prescribed SST anomalies in both experiments and in CTRL.

FIGURE 2. Two-month means of winter anomalies of 200-hPa height in the CTRL experiment (left) and corresponding TROPMLM – CTRL differences (center) and MLM – TROPMLM differences (right), for the 1997/98 NIÑO event. The contour interval is 20 m (left) and 10 m for the differences. Green and orange shading denote 95% and 99% statistical significance of the differences. The box in the left middle panel depicts the North Pacific region over which the average in Fig. 3 is taken.

FIGURE 3. a) Time series of the 30-day running means of 500-hPa height ensemble-mean anomalies averaged over a box centered in the North Pacific (32º-48ºN, 176ºE-135ºW), for all three experiments. The box is shown in Fig. 2 and is chosen so as to maximize both the NIÑO and Niña North Pacific anomaly (therefore, it is not exactly aligned with either). Solid dots and open circles indicate 95% and 99% significance of the differences between the TROPMLM and CTRL anomalies (red), the MLM and CTRL anomalies (green) and the TROPMLM and MLM anomalies (black). The month labels in the x-axis refer to day 15 of that particular month. b) Same as (a) but for NIÑO−NIÑA, or warm − cold, anomalies. c) Same as (a) but for the ensemble anomaly spread (standard deviation). Units are m.

FIGURE 4. Two-month means of winter precipitation anomalies in the CTRL

experiment (left) and differences between the TROPMLM and CTRL anomalies (right) for the 1997/98 NIÑO (top panels) and 1998/99 NIÑA (bottom panels) events. The contour interval is 0.2 cm day^{-1} for precipitation and 0.1 cm day^{-1} for the differences. Green and orange shading denote 95% and 99% statistical significance of those differences.

FIGURE 5. December 1997 anomalies of a) CTRL 200-hPa height and c) CTRL precipitation Contour interval is 20 m and 0.2 cm day-1 respectively. The remaining panels show TROPMLM – CTRL differences in b) 200-hPa height, d) precipitation, e) surface air temperature, f) surface specific humidity, g) sensible heat flux, h) latent heat flux (both positive upwards), i) SLP and j) moisture flux convergence. Contour interval is 10 m, 0.1 cm day^{-1}, 0.2 K, 0.2 g kg^{-1}, 1 W m^{-2}, 5 W m^{-2}, 0.2 hPa, and $1x10^{-5}$ g kg^{-1} s^{-1}. Shadings denotes statistical significance of the differences, as in previous figures. The purple line in panel (d) depicts the averaging region used to construct the TNWP precipitation index, and is defined by the 0.05 cm day^{-1} precipitation contour, north of 3ºN.

FIGURE 6. TROPMLM December 1997 precipitation and height anomalies stratified (composited) according to an index of precipitation averaged over the TNWP region (see purple line in Fig. 5d). The left (right) panel shows composites corresponding to the lower (upper) quartile of the TNWP precipitation index (i.e., bottom and top 25%). There are 25 individual realizations in each quartile composite. Top: total precipitation, middle: precipitation anomalies and bottom: 200-hPa height anomalies. Shadings indicate statistical significance (95% and 99% levels) of the differences between the upper and lower quartile composites. Contour interval is 0.5 cm day^{-1}, 0.2 cm day^{-1} and 20 m

respectively.

FIGURE 7. Difference between upper and lower quartile composites of precipitation, SST, surface specific humidity, 200-hPa height and sea level pressure in December 1997 in the TROPMLM experiment. Shadings indicate statistical significance (at the 95% and 99% levels). Contour interval is 0.2 cm day^{-1}, 0.1 K, 0. 25 g kg^{-1}, 20 m, and 2 hPa respectively.

FIGURE 8. Scatter plot between the December 1997 TNWP precipitation index and the 200-hPa North Pacific wavetrain index in experiments CTRL and TROPMLM. The TNWP precipitation index is defined as the total precipitation averaged over the TNWP region (area within the purple contour in Fig 5d). The 200-hPa North Pacific wavetrain index is defined as the difference between the 200-hPa anomalies averaged over the northeastern Pacific and western Pacific centers of action in Fig. 7d (areas within the -60 m contour). The number in the lower left corner indicates the correlation coefficient obtained pooling all data together. The correlation for each individual experiment is indicated in the legend box. The solid (dashed) line represents a linear (quadratic) fit to the data. The ticks dot and cross represent the ensemble-mean mean CTRL and TROPMLM values respectively.

FIGURE 9. Normalized histogram (bars) and probability density function (lines), estimated with a Gaussian Kernel, of monthly-mean December 1997 (top) and January 1998 (bottom) total precipitation (in cm day-1) averaged over the TNWP region, in the CTRL (left) and TROPMLM (right) experiments.

FIGURE 10. Left: CTRL – NEUTRAL differences in the standard deviation of early

winter (ND) and midwinter (JF) intraseasonal precipitation. Right: same but for TROPMLM – CTRL differences. Data have been band-pass filtered (with no loss of NDJF data) to retain frequencies between 6 and 45 days and the maps have been smoother with a 9-point filter. Contour interval is +/- 0.1, 0.3, 0.5, etc, cm day^{-1} (left panels) and +/- 0.05, 0.15, 0.25, etc, cm day^{-1} (right panels). The yellow (light blue) shadings indicate *variance* ratios larger than 1.25 (smaller than 0.8), which is 99% statistically significant in both cases assuming only 4 degrees of freedom per 60-day season (see also colorbar).

FIGURE 11. December and January model "climatological" (i.e. 4-year ensemble mean) SST, common to all experiments. Contour interval is 1K. The box depicts the approximate position of the TNWP region.

FIGURE 12. CTRL experiment. Upper - lower quartile composite differences of tropical precipitation (orange and purple contours) and NH extratropical 200-hPa height (red and blue contours) in December, January and February for the neutral non-NIÑO 1996/97 winter (left panel) and for the NIÑO 1997/98 winter (right panel). The index for compositing is the average of precipitation in the TNWP region. The two sets of shadings indicate statistically significant differences (95% and 99% levels). Contour interval is 0.2 cm day^{-1} and 20 m, as in Fig. 7. The sample size in each upper/lower composite is 38.

FIGURE 13**.** Left panels: Mean JFM-98 500-hPa height anomaly in the CTRL experiment (top), corresponding spread or standard deviation (middle), and signal-to-noise ratio (SNR) (bottom). Contour interval is 20 m, 20 m and 0.5. Right panels: same, but for the TROPMLM−CTRL differences (the difference between the absolute values of the SNR is shown, so that a positive difference means an increase in SNR). Contour

interval is 10 m, 10 m and 0.25. Shading in the top and middle right panels denotes statistically significant differences at the 95% and 99% confidence levels. Inset: normalized estimated PDF of JFM-1998 500-hPa height anomalies averaged over a box centered in the North Pacific (37ºN-50ºN and 150ºE-150ºW) in TROPMLM (red curve) and CTRL (blue curve).

FIGURE 14. Top: Observed regressions of December (left) and January (right) monthly precipitation rate against the North Pacific index (Trenberth and Hurrell 1994), for the period 1950-99. Contour interval is 2.5 mm. The NP index is a is a measure of the strength of the Aleutian low, with a standard deviation of 3.5 hPa in December and 4.4 hPa in January, and its sign has been reversed, for consistency with Fig 7. Bottom: Same but for SST; contour interval is 0.01 K. The datasets employed are GHCN precipitation and Reynolds SST (1994). The purple line indicates the region where the corresponding correlation is 95% statistically significant assuming one degree of freedom per year (r=+/- 0.27)

FIGURE 15. CTRL NIÑO precipitation and 200-hPa height anomalies stratified (composited) according to an index of precipitation averaged over the central equatorial Pacific (CEP). The left (right) panel shows composites corresponding to the lower (upper) quartile of this precipitation index (i.e., bottom and top 25%). Precipitation is shown in orange and purple (contour interval: 0.2 cm day^{-1}) and 200-hPa height in red and blue (20 m). Top panels: December 1997. Bottom panels: January 1998. The two sets of shadings in the right panels denote 95% and 99% statistically significant differences between upper and lower quartile composites.

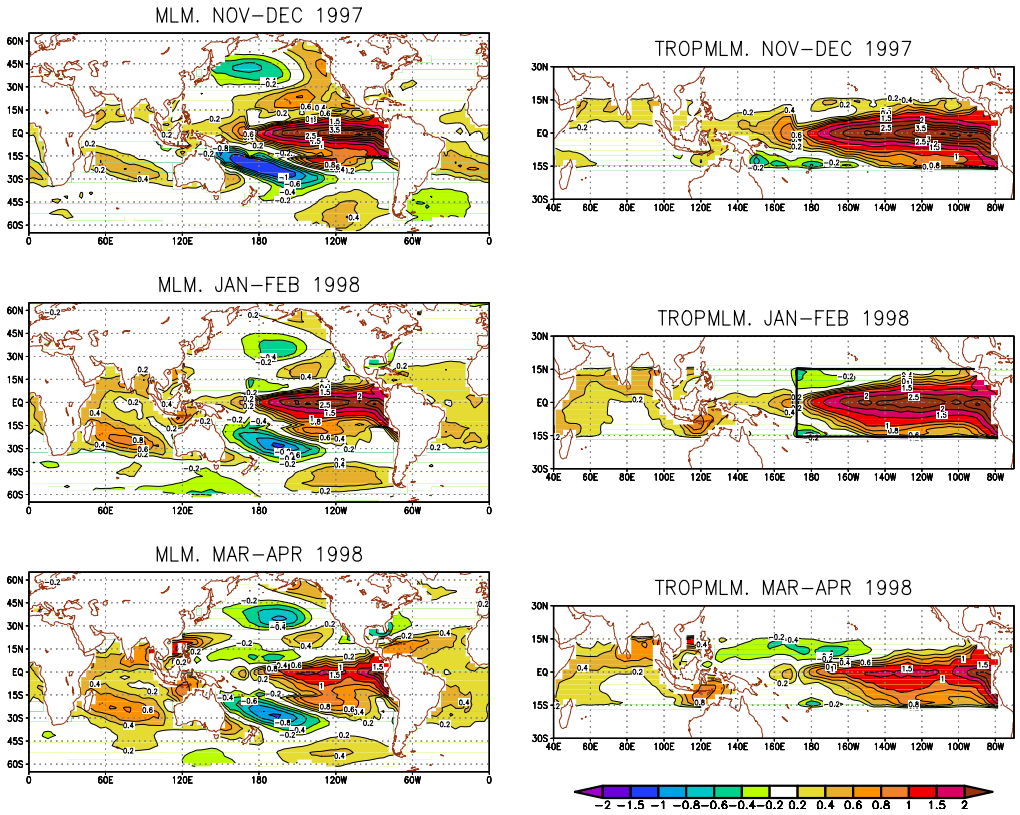

FIG 1. Two-month means of winter SST anomalies in the MLM (left) and TROPMLM (right) experiments for the 1997/98 NIÑO event. Contour interval is 0.2 ºC. The box in the middle right panel denotes the region of prescribed SST anomalies in both experiments and in CTRL.

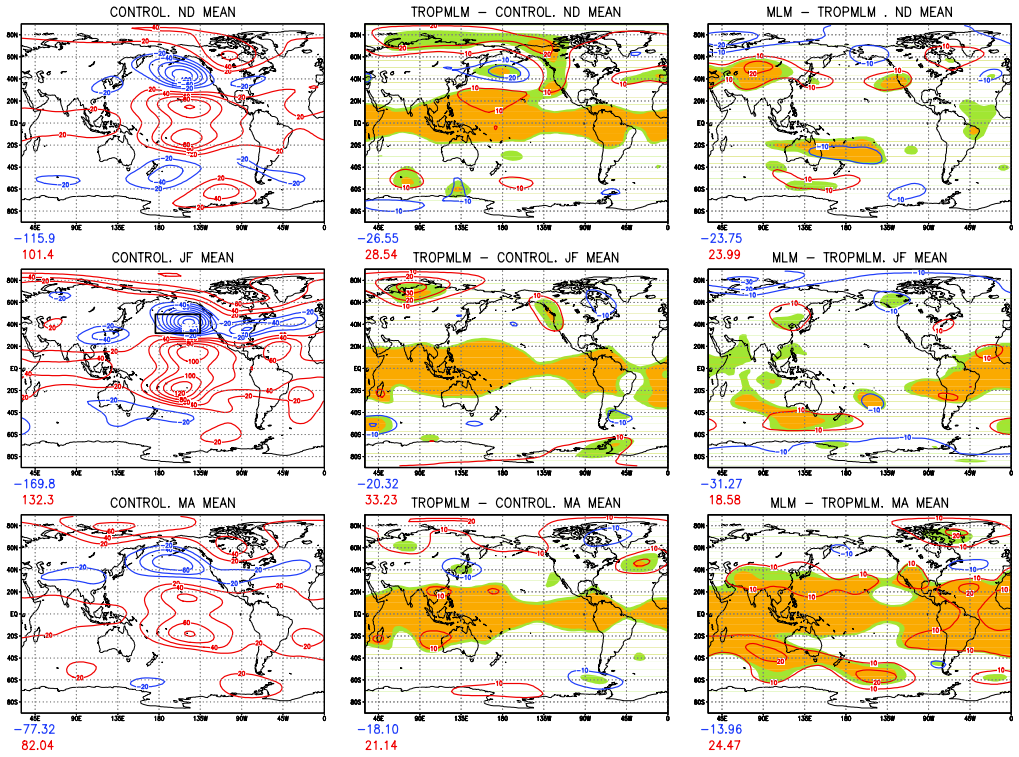

FIG 2. Two-month means of winter anomalies of 200-hPa height in the CTRL experiment (left) and corresponding TROPMLM – CTRL differences (center) and MLM – TROPMLM differences (right), for the 1997/98 NIÑO event. The contour interval is 20 m (left) and 10 m for the differences. Green and orange shading denote 95% and 99% statistical significance of the differences. The box in the left middle panel depicts the North Pacific region over which the average in Fig. 3 is taken.

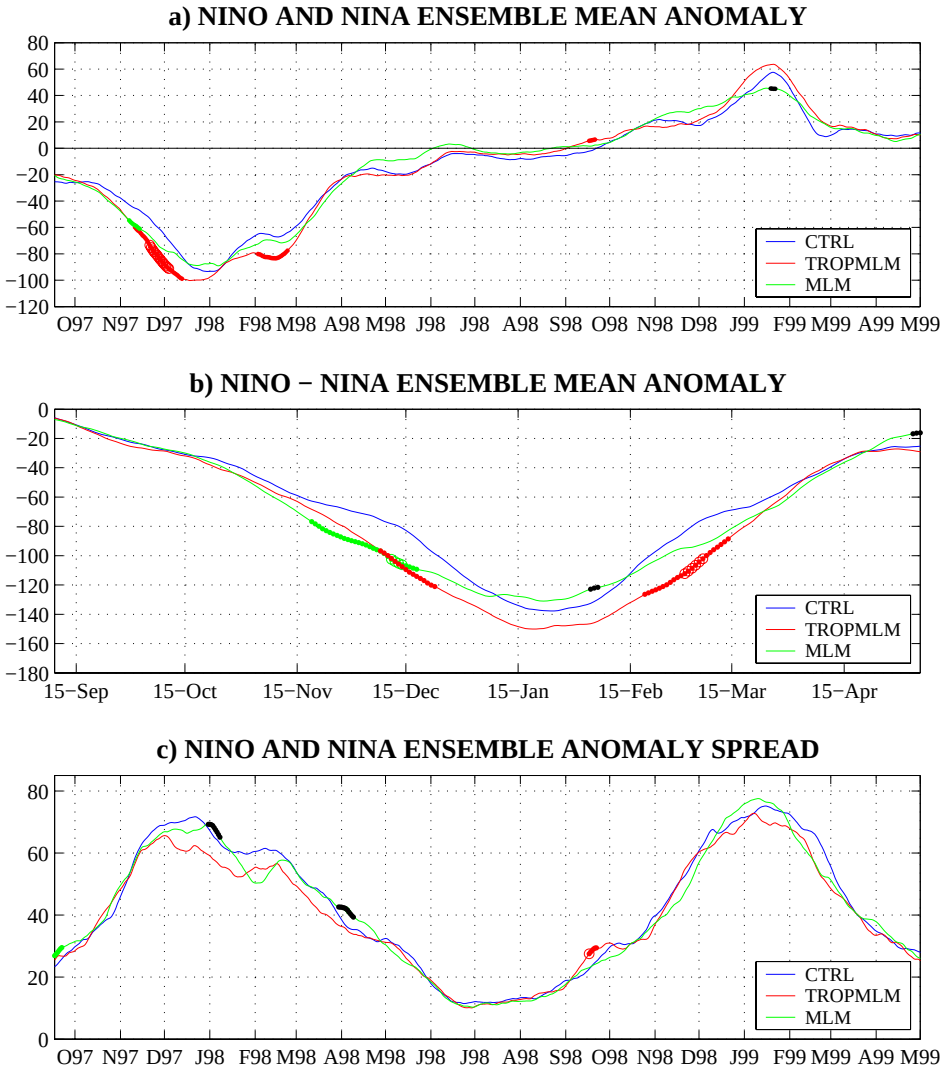

FIG. 3. a) Time series of the 30-day running means of 500-hPa height ensemble-mean anomalies averaged over a box centered in the North Pacific (32º-48ºN, 176ºE-135ºW), for all three experiments. The box is shown in Fig. 2 and is chosen so as to maximize both the NIÑO and NIÑA North Pacific anomaly (therefore, it is not exactly aligned with either). Solid dots and open circles indicate 95% and 99% significance of the differences between the TROPMLM and CTRL anomalies (red), the MLM and CTRL anomalies (green) and the TROPMLM and MLM anomalies (black). The month labels in the x-axis refer to day 15 of that particular month. b) Same as (a) but for NIÑO−NIÑA, or warm − cold, anomalies. c) Same as (a) but for the ensemble anomaly spread (standard deviation). Units are m.

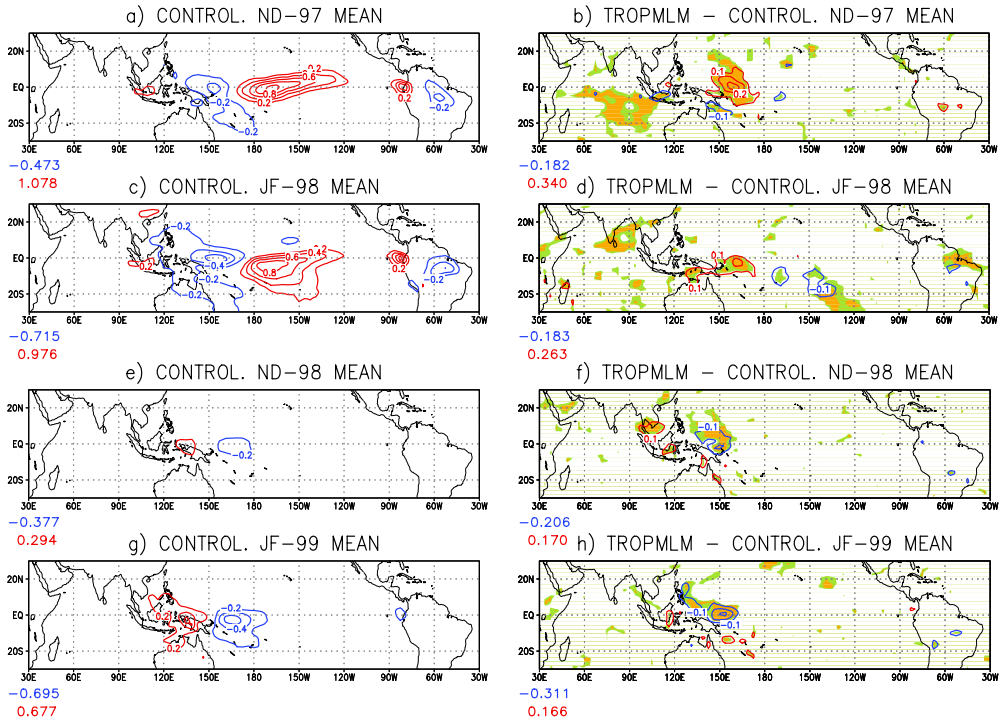

FIG. 4. Two-month means of winter precipitation anomalies in the CTRL experiment (left) and differences between the TROPMLM and CTRL anomalies (right) for the 1997/98 NIÑO (top panels) and 1998/99 NIÑA (bottom panels) events. The contour interval is 0.2 cm day^{-1} for precipitation and 0.1 cm day^{-1} for the differences. Green and orange shading denote 95% and 99% statistical significance of those differences.

DECEMBER 1997

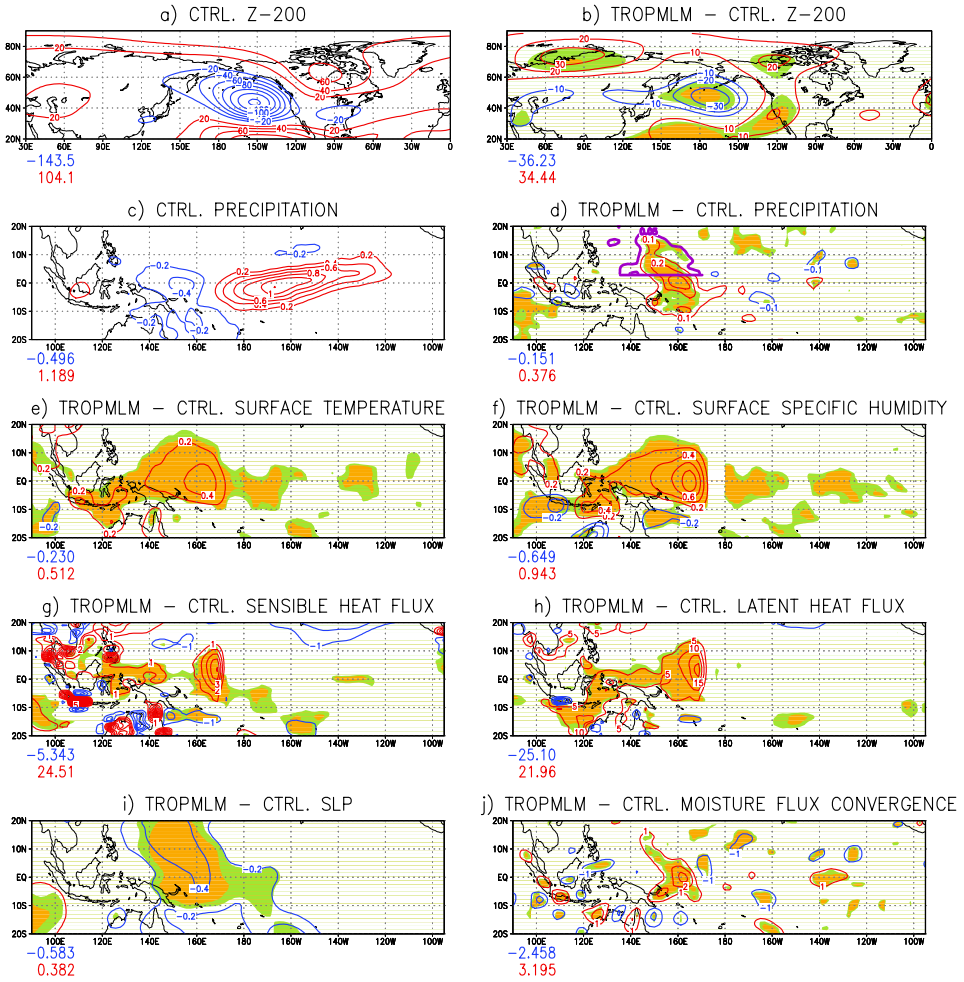

FIG. 5. December 1997 anomalies of a) CTRL 200-hPa height and c) CTRL precipitation Contour interval is 20 m and 0.2 cm day-1 respectively. The remaining panels show TROPMLM – CTRL differences in b) 200-hPa height, d) precipitation, e) surface air temperature, f) surface specific humidity, g) sensible heat flux, h) latent heat flux (both positive upwards), i) SLP and j) moisture flux convergence. Contour interval is 10 m, 0.1 cm day-1, 0.2 K, 0.2 g kg^{-1}, 1 W m^{-2}, 5 W m^{-2}, 0.2 hPa, and 1x10^{-5} g kg^{-1} s^{-1}. Shadings denotes statistical significance of the differences, as in previous figures. The purple line in panel (d) depicts the averaging region used to construct the TNWP precipitation index, and is defined by the 0.05 cm day^{-1} precipitation contour, north of 3ºN.

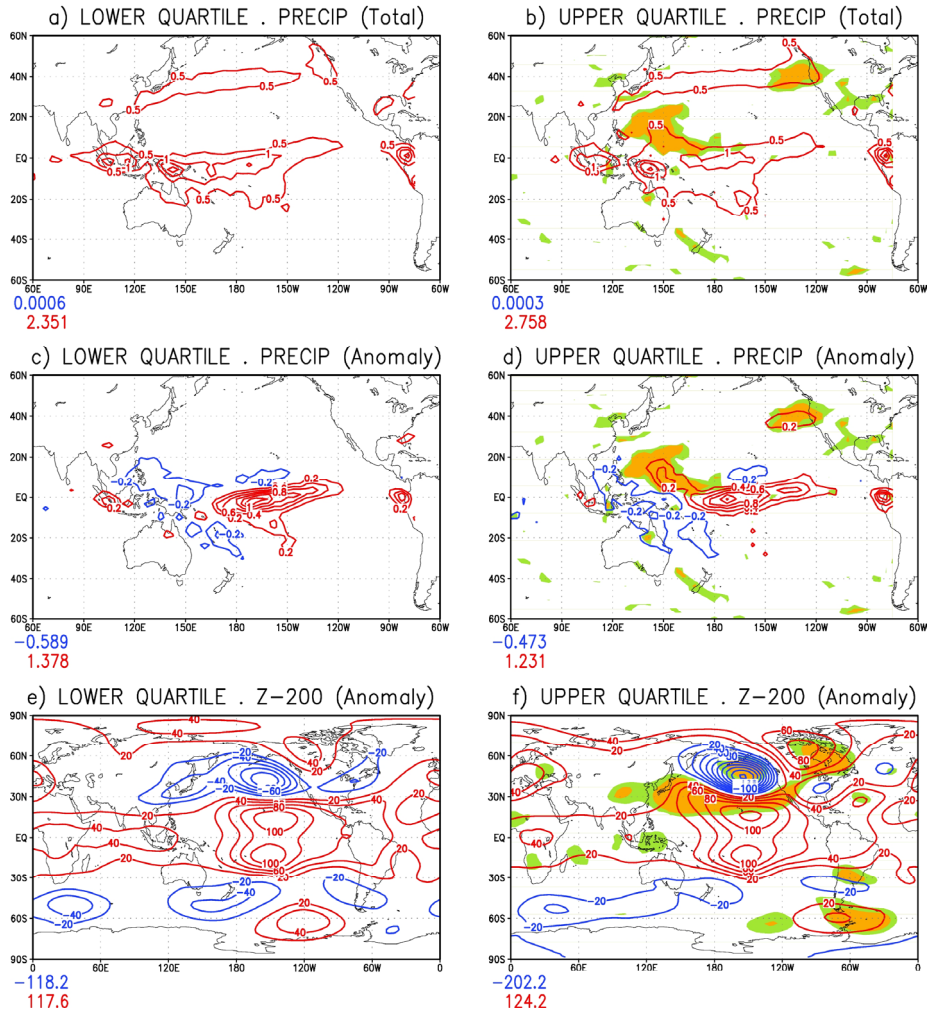

FIG. 6. TROPMLM December 1997 precipitation and height anomalies stratified (composited) according to an index of precipitation averaged over the TNWP region (see purple line in Fig. 5d). The left (right) panel shows composites corresponding to the lower (upper) quartile of the TNWP precipitation index (i.e., bottom and top 25%). There are 25 individual realizations in each quartile composite. Top: total precipitation, middle: precipitation anomalies and bottom: 200-hPa height anomalies. Shadings indicate statistical significance (95% and 99% levels) of the differences between the upper and lower quartile composites. Contour interval is 0.5 cm day^{-1}, 0.2 cm day^{-1} and 20 m respectively.

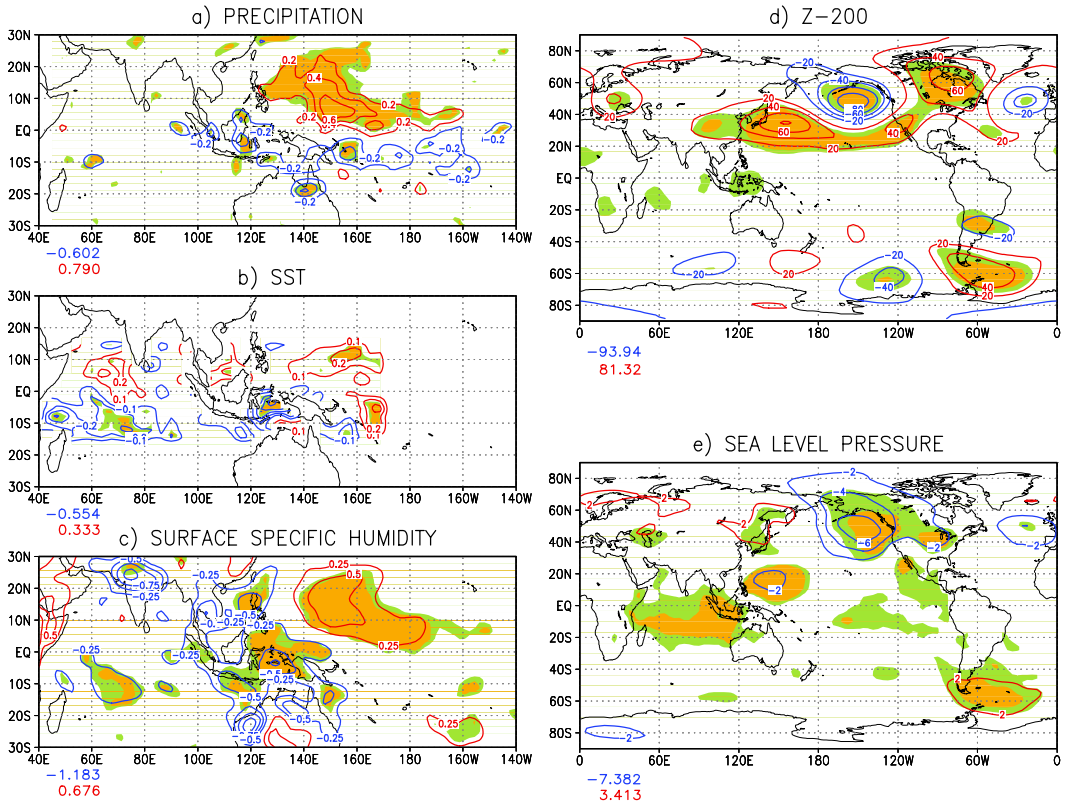

FIG. 7. Difference between upper and lower quartile composites of precipitation, SST, surface specific humidity, 200-hPa height and sea level pressure in December 1997 in the TROPMLM experiment. Shadings indicate statistical significance (95% and 99% levels). Contour interval is 0.2 cm day^{-1}, 0.1 K, 0. 25 g kg^{-1}, 20 m, and 2 hPa respectively.

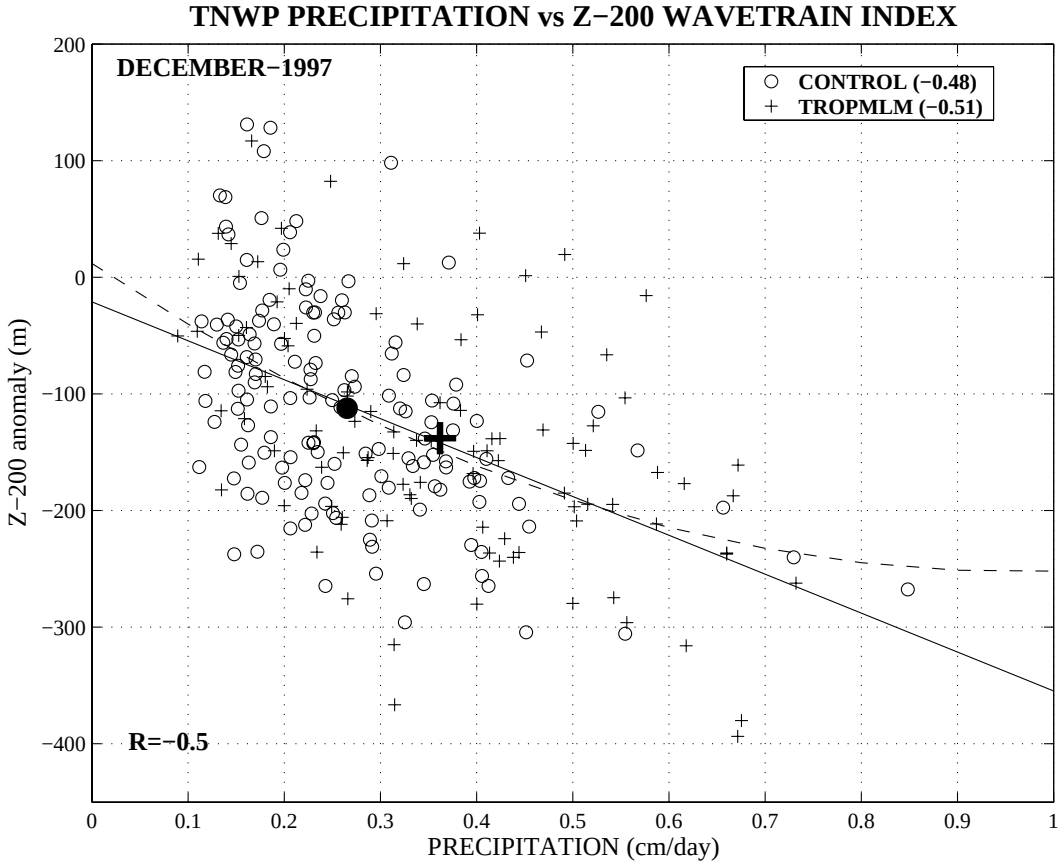

FIG. 8. Scatter plot between the December 1997 TNWP precipitation index and the 200-hPa North Pacific wavetrain index in experiments CTRL and TROPMLM. The TNWP precipitation index is defined as the total precipitation averaged over the TNWP region (area within the purple contour in Fig 5d). The 200-hPa North Pacific wavetrain index is defined as the difference between the 200-hPa anomalies averaged over the northeastern Pacific and western Pacific centers of action in Fig. 7d (areas within the -60 m contour). The number in the lower left corner indicates the correlation coefficient obtained pooling all data together. The correlation for each individual experiment is indicated in the legend box. The solid (dashed) line represents a linear (quadratic) fit to the data. The ticks dot and cross represent the ensemble-mean mean CTRL and TROPMLM values respectively.

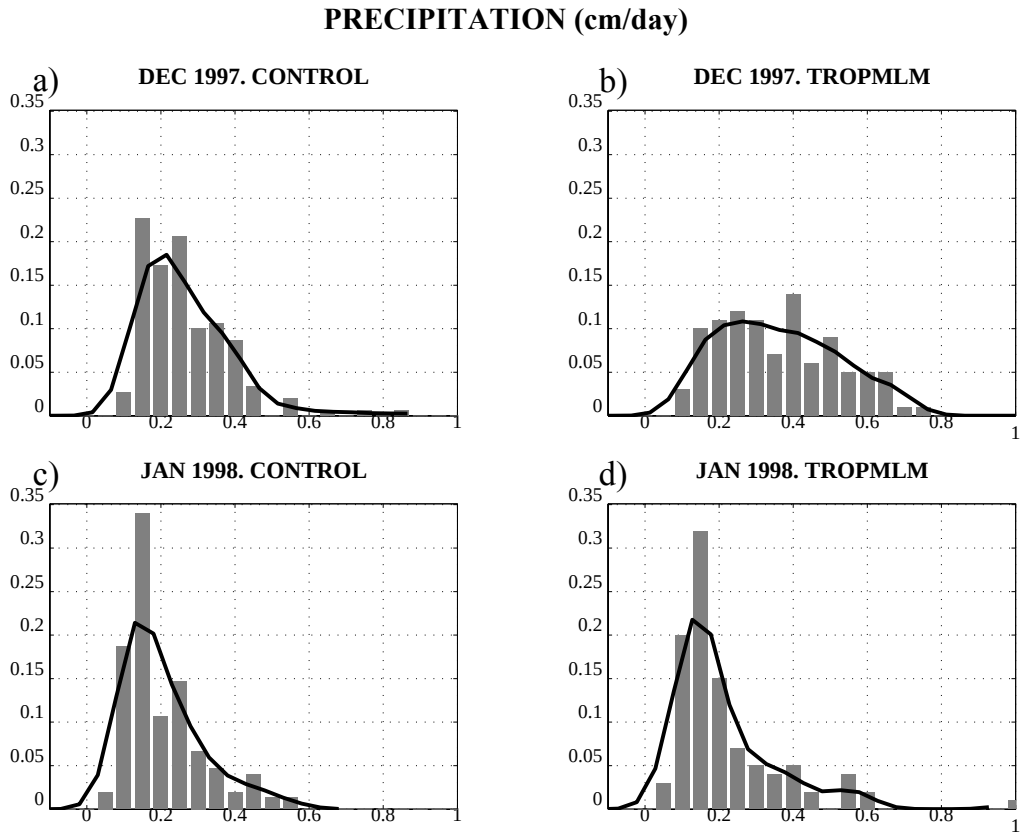

FIG. 9. Normalized histogram (bars) and probability density function (lines), estimated with a Gaussian Kernel, of monthly-mean December 1997 (top) and January 1998 (bottom) total precipitation (in cm day^{-1}) averaged over the TNWP region, in the CTRL (left) and TROPMLM (right) experiments.

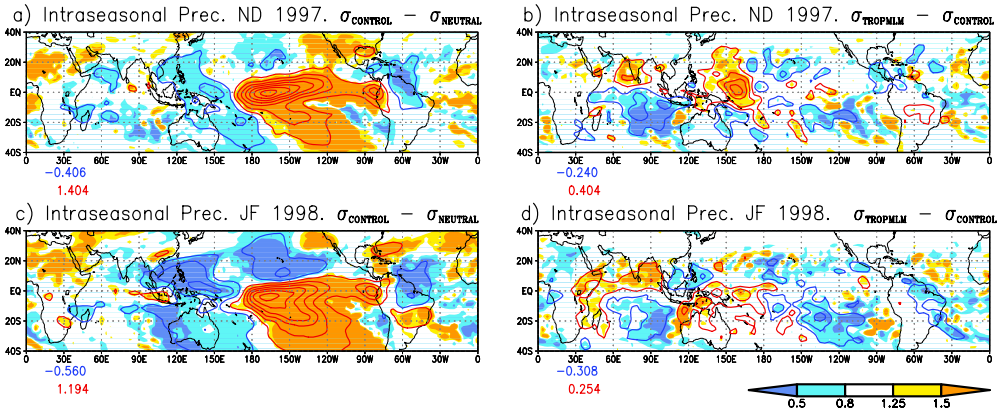

FIG. 10. Left: CTRL – NEUTRAL differences in the standard deviation of early winter (ND) and midwinter (JF) intraseasonal precipitation. Right: same but for TROPMLM – CTRL differences. Data have been band-pass filtered (with no loss of NDJF data) to retain frequencies between 6 and 45 days and the maps have been smoother with a 9-point filter. Contour interval is +/- 0.1, 0.3, 0.5, etc, cm day^{-1} (left panels) and +/- 0.05, 0.15, 0.25, etc, cm day^{-1} (right panels). The yellow (light blue) shadings indicate *variance* ratios larger than 1.25 (smaller than 0.8), which is 99% statistically significant in both cases assuming only 4 degrees of freedom per 60-day season (see also colorbar).

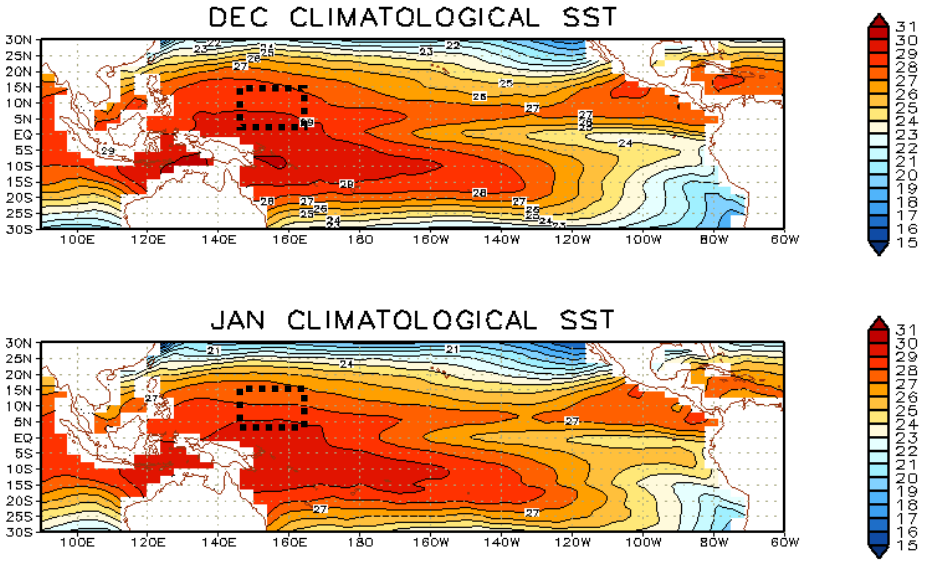

FIG. 11. December and January model "climatological" (i.e. 4-year ensemble mean) SST, common to all experiments. Contour interval is 1K. The box depicts the approximate position of the TNWP region.

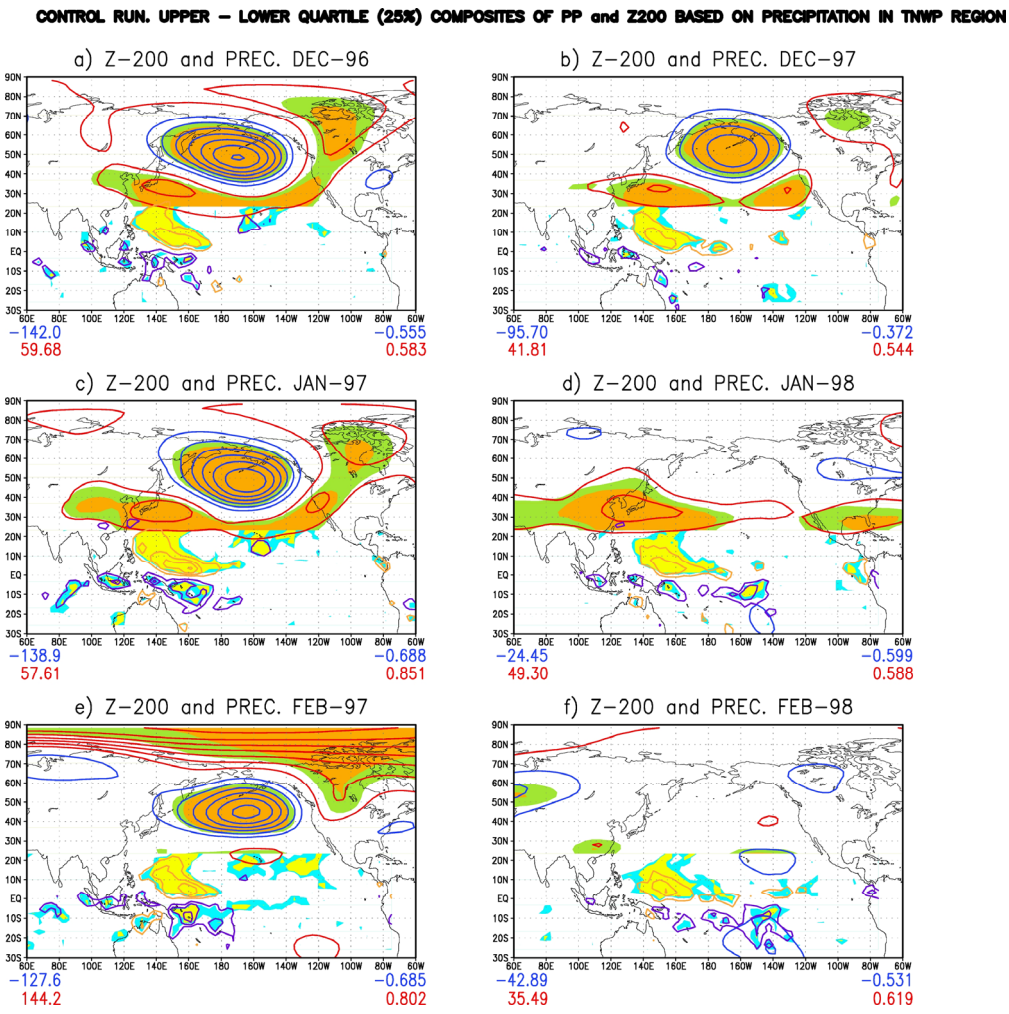

FIG. 12. CTRL experiment. Upper - lower quartile composite differences of tropical precipitation (orange and purple contours) and NH extratropical 200-hPa height (red and blue contours) in December, January and February for the neutral non-NIÑO 1996/97 winter (left panel) and for the NIÑO 1997/98 winter (right panel). The index for compositing is the average of precipitation in the TNWP region. The two sets of shadings indicate statistically significant differences (95% and 99% levels). Contour interval is 0.2 cm day-1 and 20 m, as in Fig. 7. The sample size in each upper/lower composite is 38.

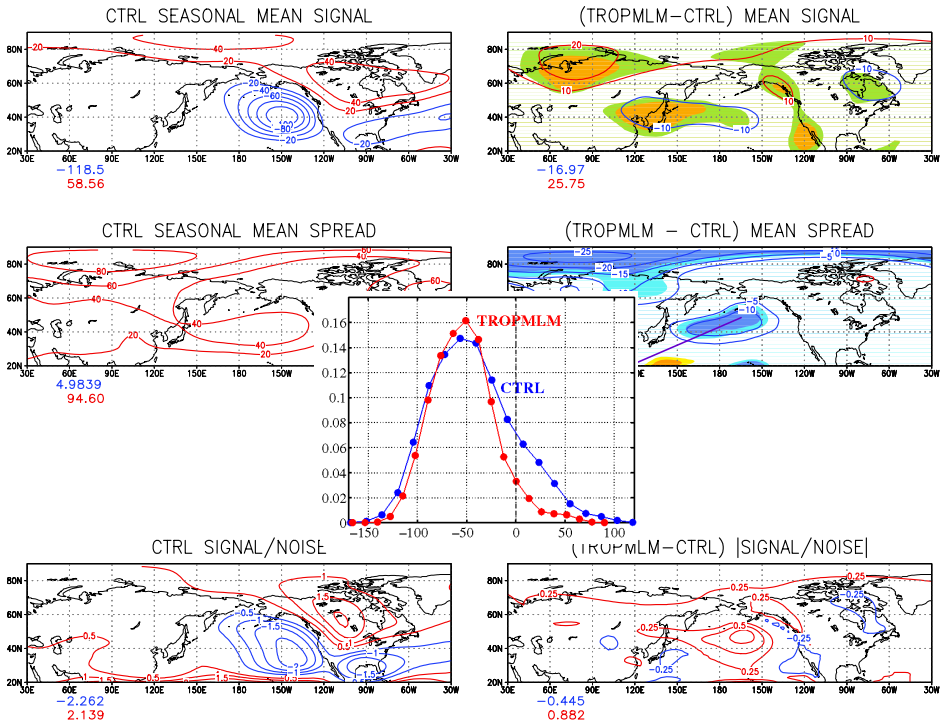

FIG. 13. Left panels: Mean JFM-98 500-hPa height anomaly in the CTRL experiment (top), corresponding spread or standard deviation (middle), and signal-to-noise ratio (SNR) (bottom). Contour interval is 20 m, 20 m and 0.5. Right panels: same, but for the TROPMLM−CTRL differences (the difference between the absolute values of the SNR is shown, so that a positive difference means an increase in SNR). Contour interval is 10 m, 10 m and 0.25. Shading in the top and middle right panels denotes statistically significant differences at the 95% and 99% confidence levels. Inset: normalized estimated PDF of JFM-1998 500-hPa height anomalies averaged over a box centered in the North Pacific (37ºN-50ºN and 150ºE-150ºW) in TROPMLM (red curve) and CTRL (blue curve).

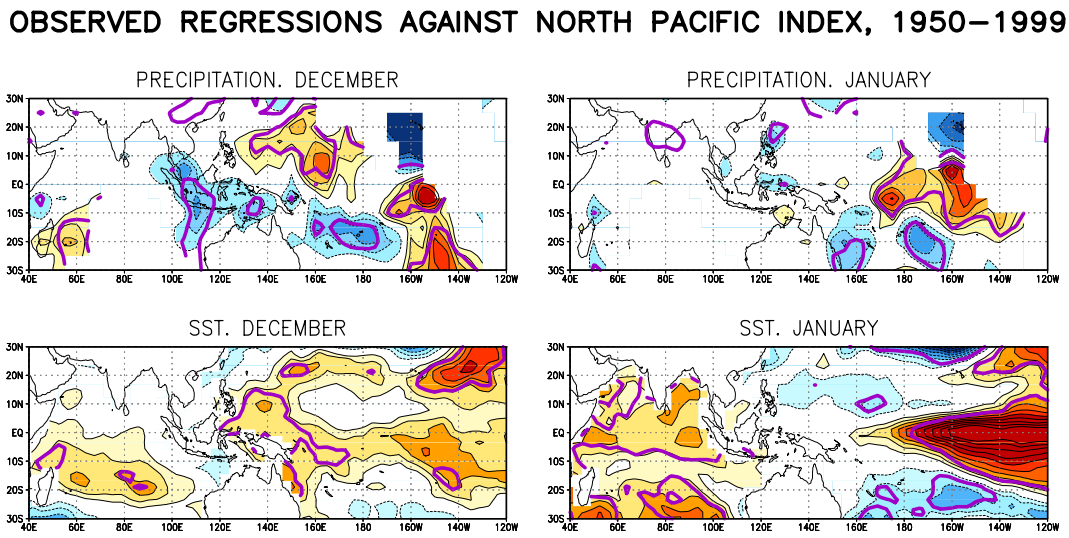

FIG. 14. Top: Observed regressions of December (left) and January (right) monthly precipitation rate against the North Pacific index (Trenberth and Hurrell 1994), for the period 1950-99. Contour interval is 2.5 mm. The NP index is a is a measure of the strength of the Aleutian low, has a standard deviation of 3.5 hPa in December and 4.4 hPa in January, and its sign has been reversed, for consistency with Fig 7. Bottom: Same but for SST; contour interval is 0.01 K. The datasets employed are GHCN precipitation, inverse area-averaged into 5x5 grid boxes (J. Escheid, personal communication), and Reynolds SST (Reynolds and Smith 1994). The purple line indicates the region where the corresponding correlation is 95% statistically significant, assuming one degree of freedom per year (r=+/- 0.27).

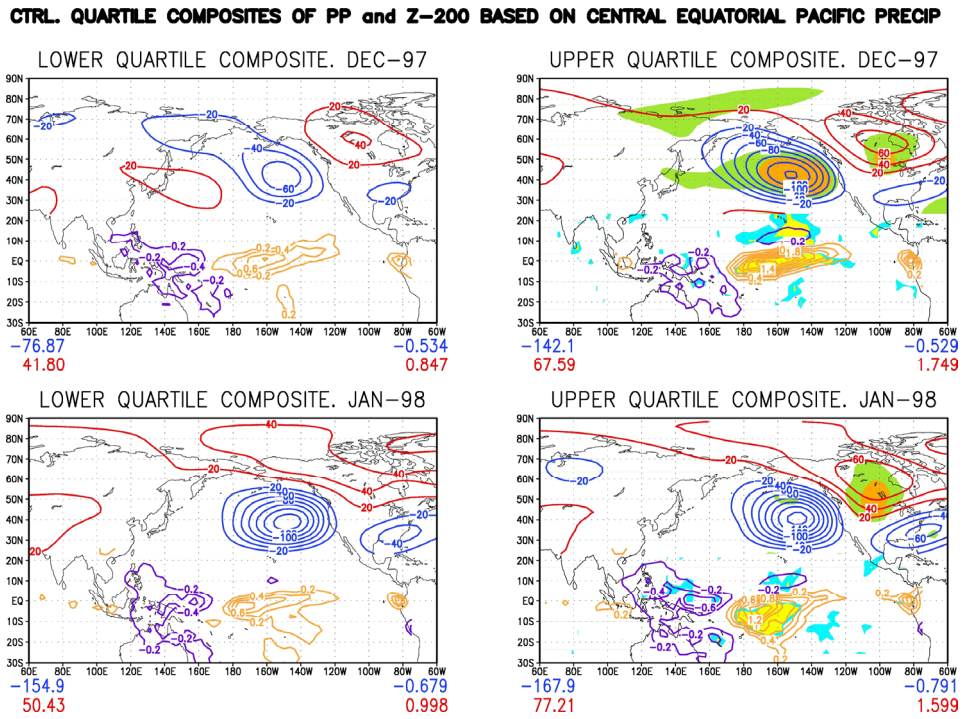

FIG. 15. CTRL NIÑO precipitation and 200-hPa height anomalies stratified (composited) according to an index of precipitation averaged over the central equatorial Pacific (CEP). The left (right) panel shows composites corresponding to the lower (upper) quartile of this precipitation index (i.e., bottom and top 25%). Precipitation is shown in orange and purple (contour interval: 0.2 cm day^{-1}) and 200-hPa height in red and blue (20 m). Top panels: December 1997. Bottom panels: January 1998. The two sets of shadings in the right panels denote 95% and 99% statistically significant differences between upper and lower quartile composites.

Table I: Description of experiments.

Experiment name	***Number of simulations***	***SST field in tropical eastern Pacific***	***Coupling configuration***[1]
NEUTRAL	150	"climatological"	no coupling
CTRL	150	observed	no coupling
TROPMLM	100	observed	coupling in tropical Indian and western Pacific oceans
MLM	150	observed	coupling in entire ice-free oceanic domain

1. "climatological" SSTs are prescribed in the uncoupled regions outside the tropical eastern Pacific